8-1-2011

IDENTIFICATION AND ANALYSIS OF PROTEINS AND GENES RESPONSIBLE FOR MICROBIAL ANAEROBIC NITRATE-DEPENDENT IRON OXIDATION AND OVEREXPRESSION IN E. coli OF PERCHLORATE REDUCTASE

Ming Gao
Southern Illinois University Carbondale, mingg@siu.edu

IDENTIFICATION AND ANALYSIS OF PROTEINS AND GENES RESPONSIBLE FOR MICROBIAL ANAEROBIC NITRATE-DEPENDENT IRON OXIDATION AND OVEREXPRESSION IN *E. coli* OF PERCHLORATE REDUCTASE

by

Ming Gao

A Dissertation Submitted in Partial Fulfillment of the Requirements for the Doctor of Philosophy Degree

Department of Molecular Biology, Microbiology, and Biochemistry

in the Graduate School

Southern Illinois University Carbondale

August 2011

IDENTIFICATION AND ANALYSIS OF PROTEINS AND GENES RESPONSIBLE FOR MICROBIAL ANAEROBIC NITRATE-DEPENDENT IRON OXIDATION AND OVEREXPRESSION IN *E. coli* OF PERCHLORATE REDUCTASE

by

Ming Gao

A Dissertation Submitted in Partial Fulfillment of the Requirements for the Doctor of Philosophy Degree

in the field of Molecular Biology, Microbiology and Biochemistry

Approved by:

Laurie Achenbach, Chair

Douglas Fix

David Clark

Judy Davie

Yanna Liang

Graduate School

Southern Illinois University Carbondale

June 29th, 2011

AN ABSTRACT FOR THE DISSERTATION OF

Ming Gao, for the Doctor of Philosophy Degree in Molecular Biology, Microbiology, and Biochemistry, presented on June 29th, 2011 at Southern Illinois University, Carbondale.

TITLE: IDENTIFICATION AND ANALYSIS OF PROTEINS AND GENES RESPONSIBLE FOR MICROBIAL ANAEROBIC NITRATE-DEPENDENT IRON OXIDATION AND OVEREXPRESSION IN *E. coli* OF PERCHLORATE REDUCTASE

MAJOR PROFESSOR: Laurie A. Achenbach

Section 1

Iron is the fourth most abundant element on the earth crust as well as an essential nutrient for all living organisms. The cycling of iron between the environment and biological systems and the microbial-mediated transformation between Fe^{2+} and Fe^{3+} has a significant impact on the biogeochemistry of the environment. The recently discovered microbially-mediated anaerobic nitrate-dependent oxidation of Fe^{2+} has been shown to play an important role in global iron biogeochemical cycling. Furthermore,

the formation of iron oxide from anaerobic nitrate-dependent Fe^{2+} oxidation results in the adsorption and precipitation of soluble toxic heavy metals and radionuclides from surrounding environment. Therefore, this metabolism has been attracting more and more attention because this process could serve as a cost-effective way to co-remediate nitrate, heavy metals and radionuclides at contaminated sites.

Little is known about the molecular genetics of the anaerobic nitrate-dependent Fe^{2+} oxidation pathway so far. Previous studies in our lab using a microarray approach on *Dechloromonas aromatica* RCB uncovered the likely involvement of lipoproteins, transmembrane proteins in major operons, cytochromes and signal transduction enzymes in this metabolism. In an effort to further elucidate the metabolic process, a recently isolated bacterium strain *Acidovorax ebreus* strain TPSY capable of anaerobic nitrate-dependent Fe^{2+} oxidation was selected as a model organism in this study. By utilizing a 2-dimensional electrophoresis method, a list of candidate proteins which exhibited elevated levels of expression were identified by the comparison of whole cell protein profile between Fe^{2+}-oxidizing strain TPSY cells and control cells.

Conserved domain analysis of the protein candidates along with the locus analysis of their corresponding genes revealed two operons (Dtpsy_1460-1463 and Dtpsy_3433-3438) that could encode key components in the anaerobic nitrate-dependent Fe^{2+} oxidation pathway. An

outer membrane efflux pump protein complex encoded by the Dtpsy_1460-1463 operon could play a role in the exportation of periplasmic-accumulated Fe^{3+} as a detoxification procedure. In addition, a putative ferric reductase protein Dtpsy_3433 and cytochrome reductase-like protein Dtpsy_3436 are likely critical electron transport chain components in this metabolism. Quantitative reverse transcription PCR provided further evidence for the involvement of this operon by demonstrating the transcriptional level up-regulation of the genes in the Dtpsy_3433-3438 operon.

This study serves as the first attempt to identify the proteins and genes responsible for anaerobic nitrate-dependent iron oxidation in *Acidovorax ebreus* strain TPSY. This work has led to the successful identification of a few key proteins and genes responsible for anaerobic nitrate-dependent Fe^{2+} oxidation, thus providing information important for the elucidation of other components in this electron transport pathway.

Section 2

Perchlorate is a wide-spread contaminant detected in drinking water and ground water systems in the United States. The current development of a highly sensitive enzymatic bioassay for *in situ* perchlorate concentration quantification created a need for high-quality and low-cost perchlorate reductase.

Perchlorate reductase, originally isolated from DPRB (dissimilatory perchlorate reducing bacteria), is encoded by an operon containing four genes, *pcrABCD*. Enzymatically active perchlorate reductase purified by traditional methods is composed of two structural subunits, PcrA and PcrB, encoded by the *pcrA* and *pcrB* genes, respectively. The lengthy traditional protein purification process and the slow growth rate of DPRB hinder the industrial mass production of this enzyme.

In this study, we report an attempt to use *E. coli* host to overexpress perchlorate reductase and use a polyhistidine tag to enable ease of the subsequent purification. The *pcrAB* genes encoding the structural subunits of perchlorate reductase were cloned into an expression vector in *E. coli.* The purification of the recombinant perchlorate reductase was performed under strict anaerobic and denaturing conditions and a highly purified form of the enzyme was obtained. Possible solutions to avoid the formation of inclusion bodies while still maintaining the enzyme activity were discussed. This work proved the feasibility of recombinant perchlorate reductase expression using an *E.coli* host and the usefulness of the histidine tag in the purification process.

In addition, this work provided insights into factors that need to be taken into future consideration in order to obtain the recombinant enzyme with full enzymatic activity. As a final goal, this study will contribute to the development of enzyme-based bioassay for the detection of perchlorate in

the environment by lowering the production and purification cost of its key component, the perchlorate reductase.

PREFACE

This dissertation consists of two sections, each of which focuses on different aspects of the manipulation and the analysis of proteins from different microorganisms.

The primary emphasis of this dissertation will be on the first section, the Identification of Proteins and Genes Responsible for Microbial Anaerobic Nitrate-Dependent Iron Oxidation. The microbial anaerobic nitrate-dependent iron oxidation has broad impact on the biochemical cycling of iron element on the earth's crust and promising applications in the bioremediation of toxic heavy metals and radionuclides. In order to understand the molecular genetics and electron transfer pathway of this metabolism, bacterium *Acidovorax ebreus* strain TPSY was used as a model organism. A combination of proteomics approach and quantitative reverse transcription PCR technique was employed to analyze key candidate proteins and their corresponding genes. With the aid of bioinformatics tools, the theoretical roles of the candidate proteins were generated and a hypothesized model of the electron transfer pathway was brought forth.

The second section represents a project conducted in my early Ph.D. program. This project focused on the overexpression in *E. coli* of perchlorate reductase from dissimilatory perchlorate-reducing bacteria. The development of a highly sensitive and cost-effective enzymatic bioassay for the *in situ* perchlorate concentration quantification created a need for high quality and

low-cost perchlorate reductase suitable for industrial application. In this section, I report an attempt to use *E. coli* host to overexpress perchlorate reductase and use a polyhistidine tag to enable ease of the subsequent purification. The successful expression and purification of the recombinant perchlorate reductase was achieved whereas the enzymatic activity could not be preserved. So further work needed for the maintenance of full enzyme activity of the recombinant perchlorate reductase was discussed.

These two sections combined represent my Ph. D. research which spans from the analysis of one target protein to the manipulation of complex protein samples in the field of microbial protein biochemistry.

TABLE OF CONTENTS

LIST OF TABLES

SECTION 1

SECTION 2

LIST OF FIGURES

SECTION 1

LIST OF FIGURES (CONTINUED)

SECTION 2

SECTION 1

ABSTRACT

Iron is the fourth most abundant element on the earth crust as well as an essential nutrient for all living organisms. The cycling of iron between the environment and biological systems and the microbial-mediated transformation between Fe^{2+} and Fe^{3+} has a significant impact on the biogeochemistry of the environment. The recently discovered microbially-mediated anaerobic nitrate-dependent oxidation of Fe^{2+} has been shown to play an important role in global iron biogeochemical cycling. Furthermore, the formation of iron oxide from anaerobic nitrate-dependent Fe^{2+} oxidation results in the adsorption and precipitation of soluble toxic heavy metals and radionuclides from surrounding environment. Therefore, this metabolism has been attracting more and more attention because this process could serve as a cost-effective way to co-remediate nitrate, heavy metals and radionuclides at contaminated sites.

Little is known about the molecular genetics of the anaerobic nitrate-dependent Fe^{2+} oxidation pathway so far. Previous studies in our lab using a microarray approach on *Dechloromonas aromatica* RCB uncovered the likely involvement of lipoproteins, transmembrane proteins in major operons, cytochromes and signal transduction enzymes in this metabolism. In an effort to further elucidate the metabolic process, a recently isolated

bacterium strain *Acidovorax ebreus* strain TPSY capable of anaerobic nitrate-dependent Fe^{2+} oxidation was selected as a model organism in this study. By utilizing a 2-dimensional electrophoresis method, a list of candidate proteins which exhibited elevated levels of expression were identified by the comparison of whole cell protein profile between Fe^{2+}-oxidizing strain TPSY cells and control cells.

Conserved domain analysis of the protein candidates along with the locus analysis of their corresponding genes revealed two operons (Dtpsy_1460-1463 and Dtpsy_3433-3438) that could encode key components in the anaerobic nitrate-dependent Fe^{2+} oxidation pathway. An outer membrane efflux pump protein complex encoded by the Dtpsy_1460-1463 operon could play a role in the exportation of periplasmic-accumulated Fe^{3+} as a detoxification procedure. In addition, a putative ferric reductase protein Dtpsy_3433 and cytochrome reductase-like protein Dtpsy_3436 are likely critical electron transport chain components in this metabolism. Quantitative reverse transcription PCR provided further evidence for the involvement of this operon by demonstrating the transcriptional level up-regulation of the genes in the Dtpsy_3433-3438 operon.

This study serves as the first attempt to identify the proteins and genes responsible for anaerobic nitrate-dependent iron oxidation in *Acidovorax ebreus* strain TPSY. This work has led to the successful identification of a few key proteins and genes responsible for anaerobic

nitrate-dependent Fe^{2+} oxidation, thus providing information important for the elucidation of other components in this electron transport pathway.

INTRODUCTION

Heavy metals and radionuclide contamination. Radionuclides are naturally-occurring metal elements in the earth's crust and mostly exist at stable and low levels that do not usually pose a public health threat. However, due to the extensive utilization of radionuclides by human activity, significant amounts of radionuclides have been released into the environment in the production of nuclear fuel, nuclear weapon testing, and the mining of uranium (60, 61). Radioactive waste produced during the nuclear fuel cycle results in soil and ground water contamination through dispersion by wind, water or leaching (60, 61). In the United States alone, the Department of Energy's nuclear installations contain 1.7 trillion gallons of contaminated ground water and 40 million cubic meters of contaminated soil, over 50% of which is comprised of radionuclides besides toxic heavy metals such as lead, chromium, and mercury (60, 61). Thus, there is an urgent need for the remediation of toxic metals and radionuclides.

The prevailing decontamination strategies nowadays are both expensive and labor intensive. A more environmental-friendly and economical approach towards the remediation of heavy metal and radionuclides would involve the use of microbially-mediated reactions that degrade or transform the toxic contaminants into less toxic compounds *in situ* without the risk of introducing additional possible contaminants.

Biological immobilization of soluble contaminants. The solubility of

heavy metals and radionuclides renders them mobile from one contaminated site to the peripheral environment through ground water movement (20), thus posing excessive challenges for remediation. Uranium is the most common radionuclide in contaminated soil and ground water and is therefore of particular concern. Uranium in contaminated sites mainly exists in the soluble U(VI) form and its property of adsorption to heterogeneous surfaces provides a method to remove U(VI) from solution by precipitation (7). Adsorption of heavy metals and radionuclides to iron oxides has been recognized as an important approach to immobilize these compounds by precipitating them into a solid form (7, 20, 31, 56, 57, 96, 111, 112). Employing the natural microbial community's ability to bio-oxidize Fe(II), the addition of Fe(II) and growth stimulating nutrition like preferred carbon source should facilitate the formation of iron oxides and result in the precipitation of heavy metals and radionuclides (57). Previous studies with *Dechloromonas* species successfully demonstrated the rapid removal of uranium and cobalt from solution during microbially-mediated iron oxide formation (57), further confirming the importance and the feasibility of the biological immobilization in the process of heavy metal and radionuclide bioremediation. Consequently, the understanding of the mechanisms and the regulatory factors involved in microbially-mediated iron oxidation becomes pivotal in order for us to fully utilize the potential of this metabolism.

Biochemical iron cycling. Iron is the fourth most abundant element in

the earth's crust (22). Its form of existence, distribution, and bioavailability exerts significant impact on the environment of living organisms. A brief model of this cycle has been recently summarized: first, microorganisms acquire iron for biochemical requirements in oxygenated, circumneutral pH environments, where the solubility of Fe(III) oxides is extremely low; second, aerobic and anaerobic autotrophic bacteria gain energy for growth from the oxidation of dissolved and solid-phase Fe(II) compounds to Fe(III) oxides; third, heterotrophic Fe(III)-reducing bacteria close the chemical loop by reducing solid-phase Fe(III) minerals back into dissolved and solid-phase Fe(II) (54). These metabolic processes are additionally coupled with the cycling of other major nutrients (e.g. carbon, oxygen, nitrogen, sulfur) and trace elements (e.g. phosphorus, nickel) (54), controlling a complicated element cycling network in a variety of environments. As an important part of the cycle, the microbial community-mediated oxidation of Fe^{2+} was described in a broad spectrum of environmental conditions (34, 53, 56, 101, 102, 114, 116-118)

Fe(II) oxidation by phototrophic Fe(II)-oxidizing bacteria.

Anoxygenic photosynthesis in the presence of Fe(II) is thought to be one of the most ancient forms of metabolism. Early studies revealed that this metabolism could be mediated by anoxygenic phototrophic bacteria (34, 43, 44, 53, 118), and *Rhodovulum iodosum* sp. nov. and *Rhodovulum robiginosum* sp. nov. were the first two reported marine phototrophic ferrous

iron-oxidizing purple bacteria strains capable of anoxygenic photosynthesis with ferrous iron as the sole electron donor (102). Studies on the molecular basis for this process in *Rhodopseudomonas palustris* TIE-1 revealed the involvement of the *pioABC* operon (48) which encodes a *c*-type cytochrome (PioA), a putative outer membrane beta-barrel protein (PioB), and a high potential iron sulfur protein. The PioA cytochrome is essential and responsible for most of the Fe(II) oxidation activity in this bacterium (48). In addition, experiments performed on *Rhodobacter* Strain SW2 suggested the involvement of another three-gene operon *foxEYZ* (25). This operon encodes a *c*-type cytochrome FoxE, a redox cofactor-containing protein FoxY, and transport function-related protein FoxZ. Through a heterologous-complementation approach, the expression of the *foxEYZ* operon was proved to enhance light-dependent Fe(II) oxidation activity (25). Notably, both of these studies highlighted the involvement of *c*-type cytochromes as important components in this metabolism. However, this type of metabolism was completely dependent on the availability of light and thus highly limited below the photic zone. Despite the significance of this metabolism to iron cycling in the earth's crust, its dependence on light highly limited its practical application to the bioremediation of soluble heavy metals and radionuclides because of the unavailability of light at most contaminated sites.

Microbially-mediated aerobic Fe(II) oxidation. Information regarding

the physiology and molecular genetics of aerobic iron oxidation metabolism were mostly obtained from studies on chemoautotrophs *Thiobacillus ferrooxidans* and *Acidithiobacillus ferrooxidans* at acidic pH with oxygen as the terminal electron acceptor (32, 35, 97, 103-105). A proteomics approach indicated the likely involvement of rusticyanin, cytochrome *c*-552, a putative phosphate binding protein, the small and large subunits of ribulose biphosphate carboxylase, and a putative CbbQ (Calvin-Benson-Bassham) protein (89). Later, iron oxidase reconstitution experiments further confirmed that the rusticyanin, cytochrome *c*, and aa_3-type cytochrome oxidase are essential for iron oxidase activity (105). However, these studies do not necessarily shed light on the mechanisms of anaerobic nitrate-dependent iron oxidation. The redox potential of Fe^{3+}/Fe^{2+} at pH 2 is +770 mV, while at pH 7 it drops to +220 mV (67), indicating a completely different biochemical pathway is involved. In addition, soluble Fe^{2+} remains stable in the presence of oxygen at low pH but primarily exists as solid-phase Fe^{2+} minerals at neutral pH (116), indicating a significantly different enzymatic activity and mechanism is required.

Microbially-mediated anaerobic nitrate-dependent Fe(II) oxidation. Only recently it was discovered that anaerobic iron oxidation could be mediated by nitrate-respiring microorganisms and this metabolism has been demonstrated in a diverse range of environments (40, 42, 56, 75, 101, 114, 116, 117). Contrary to phototrophic iron oxidation, this metabolism could

take place in the absence light so it likely exerts a greater significance on a global scale. The circumneutral iron oxidation with nitrate as the electron acceptor was first observed in a lithoautotrophic enrichment culture from brackish water sediment in Bremen, Germany (101). Since then, the discovery of a hyperthermophilic archaea capable of anaerobic iron oxidation further demonstrated the wide distribution of this metabolism in the phylogeny of life (40). Considering nitrate is usually present as a co-contaminant in heavy metal-contaminated sites (36), light-independent microbially-mediated anaerobic nitrate-dependent iron oxidation may provide a solution for the bioremediation of heavy metals and radionuclides as well as nitrate.

Fe(II)-oxidizing *Dechloromonas aromatica* strain RCB.

Dechloromonas aromatica strain RCB is a member of the β subclass of the Proteobacteria. It was originally isolated from sediments collected from Potomac River, Maryland, based on its ability to anaerobically metabolize 4-chlorobenzoate coupled to perchlorate reduction (21). Strain RCB is also capable of anaerobic benzene oxidation with NO_3^- as the electron acceptor (21) and the oxidation of reduced humic substances, Fe(II) or sulfide with the reduction of chlorate (2, 21). Strain RCB has served as a model organism in previous studies in our lab for the study of the molecular genetics of the benzene oxidation pathway, the perchlorate reduction pathway and the anaerobic oxidation of Fe(II) (Drs. Rikhi Gon and Dr.

Stacey Taft, unpublished data). In particular, a combination of microarray and RNA arbitrarily primed-PCR approach was employed by Dr. Stacey Taft to identify the genes responsible for anaerobic iron oxidation in strain RCB. The candidate genes identified from her experiments included several hypothetical proteins, lipoproteins, transmembrane proteins in major operons, cytochromes and signal transduction enzymes (S.R. Taft, unpublished data). These data provided valuable information toward further in-depth investigations into the anaerobic nitrate-dependent Fe(II) oxidation pathway.

Fe(II) oxidizing *Acidovorax ebreus* strain TPSY. *Acidovorax ebreus* strain TPSY is a motile, Gram-negative, facultative anaerobe belonging to the β subclass of the Proteobacteria. It was originally isolated from uranium- and nitrate-contaminated ground water collected from the Department of Energy ERS Field Center at Oakridge, TN. The 3.6 MB genome of strain TPSY has been sequenced and contains 3,544 candidate protein coding genes, 2701 of which have predicted functions and 958 predicted to encode enzymes (http://genome.ornl.gov/microbial/diap/). When grown anaerobically on nitrate and acetate, strain TPSY has an optimum temperature of 37^{o}C at pH 7.25 (115). Besides nitrate, it can also grow on nitrite and nitrous oxide via denitrification with the production of N_2 gas as the end product (115). In addition to its capability of anaerobic iron oxidation coupled with the reduction of nitrate at circumneutral pH, strain

TPSY is also capable of nitrate-dependent uranium oxidation and humic substances oxidation (115, 117). Strain TPSY's ability to grow mixotrophically with Fe(II) as the electron donor and nitrate as the electron acceptor in the presence of a carbon source, along with its much higher growth rate than that of *D. aromatica*, makes it a perfect model organism for the study of molecular genetics of anaerobic nitrate-dependent iron oxidation when a proteomics approach is used.

Regarding strain TPSY's ability to reduce Fe(III), limited reduction of Fe(III) to Fe(II) was observed only in the initial transfer of strain TPSY from a culture pre-grown actively on nitrate and acetate into fresh anaerobic medium amended with NTA (nitrilotriacetic acid) chelated Fe(III) as the sole electron acceptor, but continuous culturing could not be achieved under Fe(III)-reducing conditions (117). Previous work in our lab also confirmed that the amendment of Fe(III)-NTA in culture medium exerted little impact on the growth of strain TPSY compared to culture medium without any amendment (S.R. Taft. *et al*, unpublished data), suggesting that nitrate is the preferred electron acceptor when both nitrate and Fe(III) are present. In the current study, Fe(III)-NTA amendment was used as a non-iron-oxidizing environmental control.

Previous work by our lab conducted on the generation of iron-oxidizing mutant TPSY strains using transposon mutagenesis resulted in seven iron-oxidation deficient TPSY strains. Four of the seven mutants were identified to

have mutations in genes that encode an inner membrane protein, a signal transduction protein, a putative lipoprotein, and a regulatory DNA-binding protein (Dr. Stacey Taft, dissertation). The protein candidates identified from transposon mutagenesis performed on *Acidovorax ebreus* strain TPSY share significant functional similarity with the microarray assay performed on *Dechloromonas aromatica* RCB, suggesting the possible existence of a universal anaerobic nitrate-dependent iron oxidation pathway in the Proteobacteria.

Importance of this study. Since iron is the fourth most abundant element of the earth's crust and its biological cycling is closed connected to the cycling of other major elements, the iron metabolism of microorganisms has significant geological and ecological impacts. In addition, the promising bioremediation of heavy metals and radionuclides by the binding to iron oxides underscores the urgent need for understanding the anaerobic nitrate-dependent iron oxidation mechanism. However, little information regarding the molecular genetics of this pathway has been obtained so far. Identifying the key proteins and genes in the anaerobic nitrate-dependent iron oxidation pathway will be the first step towards the elucidation of this metabolism at the molecular level, thus enabling better regulation and optimization of the *in situ* bioremediation of heavy metals and radionuclides.

Here we demonstrate a proteomics approach to screen for proteins responsible for anaerobic nitrate-dependent Fe^{2+} oxidation in strain TPSY.

Protein candidates recognized by 2-D electrophoresis method along with their corresponding genes were identified and further subjected to functional analysis using bioinformatics tools. We provide evidence for the involvement of a few key gene products that may be critical components in the metabolism and present a molecular model that describes the roles of those gene products in anaerobic iron oxidation.

MATERIALS AND METHODS

Bacterial strain and growth conditions. *Acidovorax ebreus* strain TPSY cells were grown in anaerobic PIPES-buffered fresh medium (5 mM ammonium chloride, 5 mM sodium phosphate dibasic, 1 mM potassium chloride, 20 mM PIPES disodium salt, 1% Wolfe's vitamin solution, 1% Wolfe's mineral solution, 12 mM sodium nitrate, 6.25 mM sodium acetate, pH 7.0). The growth medium was amended with ferrous iron in nitrilotriacetic acid (Fe(II)-NTA, 2 mM, added from anaerobic stock) as the Fe(II)-oxidizing environment or ferric iron in nitrilotriacetic acid (Fe(III)-NTA, 2 mM, added from anaerobic stock) as the non-iron oxidizing control. A 10% inoculum of anaerobically-grown strain TPSY was added to a 2-L rubber stopper-secured bottle containing 500 ml PIPES-buffered fresh medium and incubated at 37^{o}C. Cell growth was monitored by measuring absorbance at 600 nm and Fe(II) oxidation was observed by the color change of the iron in the medium which changed from a pale yellow-greenish to orange and, finally, brown. The absorbance from the formation of Fe(III) was determined using medium after the removal of cells and subtracted from the total reading. Cells were harvested at mid-log phase by centrifugation (5000×g, 15 min) at 4^{o}C and washed twice in cold TBS buffer (50 mM Tris, 150 mM NaCl, pH 7.4). Cell pellets were immediately stored at -80^{o}C for whole cell

protein extraction. For RNA extraction, 100-µg cell pellets were resuspended in 1 ml RNA*later* solution (Ambion) and stored at 4^{o}C overnight before being stored at -80^{o}C.

Cell lysis and protein extraction. Cell pellets (100 mg) were allowed to thaw on ice and were then resuspended in 1 ml sample rehydration buffer (7 M urea, 2 M thiourea, 1% ASB-14 detergent, 40 mM Tris base, 0.001% bromophenol blue, 0.2% Bio-lyte pH3-10 ampholyte (Bio-Rad), 1×protease inhibitor (Roche)). Total proteins were released from cells by ultrasonic disruption at mid-intensity for 10×15 sec burst.

Protein sample reduction and alkylation. Protein sample reduction and alkylation were performed using the ReadyPrep Reduction-Alkylation Kit (Bio-Rad). Briefly, Alkylation Buffer (30 µl) was added to 1 ml crude protein sample to adjust the pH of the sample to between 8 and 9. TBP (tributylphosphine) (25 µl) was added to a final concentration of 5 mM and the mixture was incubated at room temperature for 30 min. Then 0.5 M iodoacetamide (30 µl) was added to a final concentration of 15 mM and the mixture was incubated for 1 hr. An additional 25 µl TBP was added to the above mixture and incubated for 15 min to quench any excessive iodoacetamide. Insoluble material was pelleted by centrifugation at 12,000×g for 30 min at 4^{o}C. The supernatant was aliquoted in 100 µl aliquots in 1.5-ml microcentrifuge tubes.

Protein sample cleanup. Protein sample cleanup was performed using

the ReadyPrep 2-D Cleanup Kit (Bio-Rad). In a 1.5-ml microcentrifuge tube, Precipitation Agent 1 (300 µl) was added to 100 µl protein sample, mixed well by vortexing, and incubated on ice for 15 min. Then Precipitation Agent 2 (300 µl) was added to the mixture of protein and Precipitation Agent 1, mixed well by vortexing, and centrifuged at 12,000×g for 5 min to form a tight pellet. Without disturbing the pellet, the supernatant was removed by pipet. Any residual liquid was collected at the bottom of the tube by centrifugation for another 30 sec and removed by pipet. Wash Reagent 1 (40 µl) was added on top of the pellet followed by centrifugation at 12,000×g for 5 min; the wash was removed by pipet. ReadyPrep proteomic grade water (Bio-Rad) (25 µl) was added on top of the pellet and the tube was vortexed for 20 sec. Wash Reagent 2 at -20^{o}C (1 ml) was added into the tube and mixed well by vortexing for 1 min. The tube was then incubated at -20^{o}C for 30 min while vortexing for 30 sec every 10 min during the incubation period. After incubation, the tube was centrifuged at 12,000×g for 5 min to form a tight pellet. Supernatant was discarded and the pellet was allowed to air-dry at room temperature for 3 - 5 min. The protein pellet was resuspended in 75 µl sample rehydration buffer. Protein samples were stored at -80^{o}C until use.

Protein concentration determination. Protein concentrations were determined using the 2-D Quant Kit (GE healthcare). Prior to performing the assay, a working color reagent was prepared by mixing 10 ml Color Reagent A and 100 µl Color Reagent B. A standard curve of protein amount from 0 µg

to 50 µg was prepared using 2 mg/ml Bovine Serum Albumin (Table 1). Protein sample (1-10 µl) containing 1-50 µg protein was added to a 1.5-ml microcentrifuge tube. To each tube (including the standard curve tubes), Precipitant (500 µl) was added to the protein sample, mixed well by vortexing, and incubated at room temperature for 3 min. Co-precipitant (500 µl) was then added to each tube and mixed briefly by vortexing or inversion. The tubes were centrifuged at ≥ 10,000×g for 5 min (with the cap-hinge facing outward) to sediment the protein and immediately removed from the centrifuge as soon as the centrifugation was complete.

Table 1: Preparation of standard curve

Tube number	1	2	3	4	5	6
Volume of 2 mg/ml BSA solution	0 µl	5 µl	10 µl	15 µl	20 µl	25 µl
Protein quantity	0 µg	10 µg	20 µg	30 µg	40 µg	50 µg

After the supernatant was decanted, the tubes were centrifuged again for 5-10 sec (with the cap-hinge facing outward) to bring any remaining liquid to the bottom of the tube. The remaining supernatant was carefully removed by using a pipet. With no visible liquid remaining in the tubes, Copper Solution (100 µl) and de-ionized water (400 µl) were added to the tube to dissolve the precipitated protein by vortexing. Working Color Reagent (1 ml) was added to each tube and instantaneous mixing was achieved by introducing the reagent as rapidly as possible. The tubes were

incubated at room temperature for 17 min. Using water as reference, absorbance readings were taken at 480 nm for each tube. A standard curve was generated by plotting the absorbance of standards against the corresponding quantity of the protein. Target protein concentration was determined by plotting the absorbance reading to the standard curve.

First dimensional isoelectricfocusing (IEF). Sample rehydration buffer (300 µl) with TBP (tri-butylphosphine, 1%) was added as a line along the edge of each channel except for about 1 cm at each end in a new rehydration/equilibration tray (Bio-Rad). After the cover sheet was peeled off using forceps, IPG (immobilized pH gradient) (Bio-Rad, 17 cm, pH 3-10, pH 4-7, pH 5-8, or pH 7-10) strips were gently placed, gel side down, onto the sample rehydration buffer in the channel. Care was taken not to introduce air bubbles beneath the IPG strips. Mineral oil (Bio-Rad) (2.5 ml) was added to each channel by carefully dripping the oil onto the plastic backing of the IPG strips while moving the pipet along the length of the IPG strips to prevent evaporation during the rehydration process. The rehydration/equilibration tray was covered with the plastic lid provided and left on a level bench for 11-16 hours to rehydrate the IPG strips.

After rehydration was complete, IPG strips were removed from the rehydration/equilibration tray and the excess mineral oil was removed by blotting the IPG strips on filter paper wetted with deionized water. The rehydrated IPG strips were placed, gel side up, in the cup loading tray (Bio-

Rad) with the anode end flush against the anode side of the cup loading tray. Two paper wicks (Bio-Rad), each wetted with 10 µl deionized water, were placed onto the gel surface at the ends of the IPG strips. Movable electrode assemblies (Bio-Rad) were placed at the cathode and anode ends of the IPG strips over the paper wicks. Good contact between the electrodes and the electrode contact areas on the front of the cup loading tray was confirmed. Small sample cups (Bio-Rad) were securely positioned on the gel surface near the anode end of the IPG strips. Protein samples containing 120 µg (for pH 4-7, pH 5-8, and pH 7-10 IPG strips) or 60 µg (for pH 3-10 IPG strips) total protein was added into each sample cup. Each sample and IPG strip was overlaid with mineral oil. The cup loading tray with the properly positioned electrodes and sample cups was placed onto the PROTEAN IEF cell apparatus. IEF was performed at 20^{o}C with a maximum current of 50 µA per IPG strip, employing the following voltage profile: rapid increase from 0 V to 10,000 V for 75,000 Vh (for pH 4-7, pH 5-8, and pH 3-10 strips) or 90,000 Vh (for pH 7-10 strips).

Equilibration and SDS-PAGE. After the completion of the IEF, the IPG strips were removed from the cup loading tray and transferred to a new rehydration/equilibration tray. The remaining mineral oil on the IPG strips was removed by placing the IPG strips on a piece of dry filter paper and blotting with a second piece of wet filter paper as previously described. SDS-PAGE Equilibration Buffer I (6 M urea, 0.375 M Tris-HCl, pH8.8, 2% SDS, 20%

glycerol, 2% DTT(Dithiothreitol)) (6 ml) was added to each IPG strip-containing channel of the rehydration/equilibration tray. The tray was then placed on an orbital shaker and gently shaken for 10 min. At the end of the 10 min incubation, equilibration buffer I was carefully discarded by decanting. SDS-PAGE Equilibration Buffer II (6M urea, 0.375 M Tris-HCl, pH 8.8, 2% SDS, 20% glycerol, 2.5% iodoacetamide) (6 ml) was added to each IPG strip-containing channel. The tray was returned to the orbital shaker for 10 min. At the end of the incubation, equilibration buffer II was discarded by decanting. Each IPG strip was removed from the rehydration/equilibration tray and dipped briefly into a 100-ml graduated cylinder containing 1× TGS running buffer (diluted from 10× TGS running buffer, Bio-Rad) and transferred, gel side up, onto the back plate of a precast 12%-20% gradient SDS-PAGE gel (Jule Biotechnologies, Inc.) above the IPG well. For each SDS-PAGE gel, pre-melted Overlay Agarose Solution (Bio-Rad) (1 ml) was added into the IPG well of the gel and the IPG strip was pushed into the IPG well before the agarose solidified. The agarose was allowed to solidify for 5 min. The SDS-PAGE gels with inserted IPG strips were then mounted into the PROTEAN II XL electrophoresis apparatus. SDS-PAGE was performed under the following electrophoresis conditions: 16 mA per gel for 30 min, then 24 mA per gel for 5.5 hr. Following electrophoresis, the SDS-PAGE gels were separated from the glass plates and stained in 200 ml Oriole Fluorescent Gel Stain (Bio-Rad) in a glass gel-staining tray on an orbital shaker for 90 min.

At the end of the staining period, gels were rinsed in 200 ml deionized water for 5 min. Gel images were captured and documented using a Gel Doc system equipped with Quantity One Analysis software (Bio-Rad).

Protein identification and conserved domain search. Protein spot detection, matching and replicate gel analysis were conducted using the PDquest 2-D Analysis software program (Bio-Rad). Protein spots of interest were excised from the gels using clean scalpels and stored in a 2-ml microcentrifuge tube containing 200 µl ReadyPrep Proteomics Grade Water (Bio-Rad) until use. Protein identification using LC/MS/MS and Peptide Mass Fingerprint was performed by Midwest Bio Services, LLC (Kansas, USA) and the SIUC Mass Spectrometry Facility (Southern Illinois University, Carbondale, IL), respectively. Conserved domain search and protein sequence similarity alignment was conducted using public-domain software (http://www.ncbi.nlm.nih.gov/Structure/cdd/wrpsb.cgi).

RNA extraction. All pipettes, plastic tips and tubes were either purchased as nuclease-free or treated with RNase*Zap* (Ambion). All reagents were prepared with sterilized DEPC (diethyl pyrocarbonate, 0.1%)-treated water. Total RNA extraction was performed using TRIzol reagent (Invitrogen). Strain TPSY cells (10 mg after the removal of RNA*later* solution by centrifugation) were resuspended in 1 ml TRIzol reagent and vortexed. The cell suspension was transferred to a 2-ml Lysing Matrix B (MP Bio) tube and homogenized in a FastPrep biopulverizer (MP Bio) for 30 seconds.

Immediately after homogenization, 200 µl chloroform was added and the tube was shaken by hand for 15 seconds. The sample was incubated at room temperature for an additional 2 min and then centrifuged at 12,000×g for 15 min at 4^{o}C. The resulting upper aqueous phase was transferred to a fresh tube and the RNA was then precipitated by adding cold isopropyl alcohol (500 µl). The mixture was incubated again at room temperature for 10 min and centrifuged at 12,000×g for 15 min at 4^{o}C. The RNA pellet on the bottom of the tube was washed once with 1 ml cold 75% ethanol centrifuged at 12,000×g for 5 min at 4^{o}C. After the ethanol was removed by using a pipet, the tube was placed upside down to air-dry the RNA pellet for 5 min. Finally, the pellet was resuspended in 50 µl nuclease-free water.

DNase treatment. RNA samples were treated with the TURBO DNA-*free* kit (Ambion) to remove residual DNA contamination. Briefly, 0.1 volume of 10× TURBO DNase buffer (5 µl) and 1 µl DNase were added to the 50 µl RNA sample, mixed gently, and incubated at 37^{o}C for 30 min. At the end of the incubation, 0.1 volume of the DNase Inactivation Reagent (5 µl) was then added to the mixture, vortexed, and incubated for 2 min. The DNase Inactivation Reagent was pelleted to the bottom of the tube by centrifuge at 7,500×g for 5 min. Avoiding the Inactivation Reagent, the supernatant was carefully transferred to a fresh tube.

The RNA concentration was determined using a spectrophotometer. 1 µl of RNA sample was diluted 100 fold in 99 µl DEPC-treated water and

transferred to a quartz cuvette, where the A_{260} and A_{280} measurements were recorded. Pure RNA yields an absorbance ratio (A_{260}/A_{280}) of 1.9 - 2.1. RNA integrity was also analyzed by agarose gel electrophoresis and ethidium bromide staining. Pure RNA would display two distinct ribosomal RNA bands (23S and 16S) without showing any smearing or a collection of small RNAs and 5S towards the bottom of the gel. Degraded or contaminated RNA could show significant smearing and distorted ribosomal RNA bands.

Reverse transcription. First-strand cDNA was synthesized using a modified protocol of ImProm-II Reverse Transcription System (Promega). All preparation steps were performed on ice unless otherwise specified. In a 20-µl RNase free tube, RNA sample containing 1.5 µg total RNA, 300 ng random hexamers (Roche) and nuclease free water were added to a final volume of 5 µl. The content was mixed using a pipet. The RNA and random primers were denatured by putting the tube in a thermocycler using the following program conditions: 70^{o}C for 5 min and 4^{o}C for 5 min. A master mix (15 µl) containing nuclease free water (6.1 µl), ImProm-II 5× Reaction Buffer (Promega) (4 µl), $MgCl_2$ (25 mM, 2.4 µl), dNTP mix (1 µl), RNasin Inhibitor (0.5 µl) and ImProm-II Reverse Transcriptase (Promega) (1 µl) was prepared and added to the tube immediately after the denaturation program, mixed by vortexing and kept on ice. The tube containing the 20 µl cDNA synthesis reaction mixtures was put in a thermocycler and the following program was used: 25^{o}C for 5 min then 37^{o}C for 60 min; reactions were

terminated by heating at 70°C for 15 min. The cDNA solutions were diluted 10-fold and stored at -20°C before PCR amplification.

Preparation of DNA primers. Sequence information for each gene of interest was obtained from the *Acidovorax ebreus* strain TPSY annotated gene database (http://genome.jgi-psf.org/dia_t/dia_t.home.html). The least conserved sequences in each target gene were chosen in order to avoid unspecific amplification during PCR. Gene-specific primer pairs (Table 2) were designed using MacVector 8.0 (Oxford Molecular Group). Primer pair specificity was further examined using BLAST (http://blast.ncbi.nlm.nih.gov/Blast.cgi).

Quantitative real-time PCR. Real-time PCR amplification was performed using IQ SYBR Green Supermix (Bio-Rad). For each reaction, 1 µl of previously prepared cDNA sample was added as template, 1 µl of each primer was added to give a final concentration of 200 nM, 25 µl iQ SYBR Green Supermix (Bio-Rad) and 22 µl sterile water were added to bring the final volume to 50 µl. The reactions were then transferred into the wells of a Low-Profile 48-Well Unskirted PCR Plate (Bio-Rad). Two replicates were included for each gene as shown in the plate layout (Table 3). The amplification was performed by putting the plate in a MiniOpticon Real-Time PCR Detection System (Bio-Rad) using the following cycling conditions: initial denaturation and polymerase activation at 95°C for 3 min followed by 40 cycles of denaturation at 95°C for 30 s, annealing at 60°C for 30 s, and

extension at 72^{o}C for 30 s with fluorescence reading at the end of the extension. At the end of each run, a melting curve was generated by ramping the reaction from 60^{o}C to 96^{o}C with a fluorescence read every increment of 0.5^{o}C. Only one sharp melting peak was observed for all samples, indicating the absence of unspecific PCR products. NTC (No template control) was conducted for each sample with each primer pair to exclude interference resulting from primer-dimer formation. The specificity of the qRT-PCR reaction was further confirmed by gel electrophoresis of end-point PCR products. Amplification efficiency was automatically calculated (CFX manager software, Bio-Rad) by generating a standard curve using a 10-fold serial dilution of cDNA template for each primer set based on the formula described by Pfaffl (87). A correlation coefficient (R^2) ≥ 0.99 for each standard curve was confirmed before an efficiency value was considered valid. The expression level of the GOI (gene of interest) was normalized to the expression level of an internal reference (16S rRNA) according to the model outlined by Vandesompele et al. (110). Normalized expression of GOI relative to control was automatically calculated using CFX Manager software (Bio-Rad).

Table 2. Primers used in qRT-PCR analysis.

Gene	Primer direction	Sequence (5'-3')	Efficiency (%)
Dtpsy_3433	Forward	GGCGAGATGGCTTTTTACCTG	96.5
	Reverse	AGCGGGAGCGTCCAGAAGG	
Dtpsy_3434	Forward	TGAAATACCCGACCCCGTTGC	92.3
	Reverse	CGCACTTCGTAGCAGCCGTC	
Dtpsy_3435	Forward	TCCCACACCAAACCCCTGCTG	96.3
	Reverse	TGAGGTAGACGGCGAGGTAGG	
Dtpsy_3436	Forward	GAAATCCGCCACCTGCCCTCC	86.5
	Reverse	CCCCGAGACCGAGAGCACCAG	
Dtpsy_3437	Forward	GGAAAGCCCCGAGACCTGCC	90.8
	Reverse	AGCGTGACCAGTCCGTTGCC	
Dtpsy_3438	Forward	CGCACCACCTTCTCTCTCGCC	92.0
	Reverse	CGAAAAATACTGCCACCCGTG	
Dtpsy_1463	Forward	AGGACAACCACGAACTGGAG	92.9
	Reverse	AGACGTAGACCCCCAGCAC	
Dtpsy_1074	Forward	TTCTCCCACGCCAACAGTTTC	92.8
	Reverse	CAGCCATCACGCTCAGGAAGC	
Dtpsy_1447	Forward	ACCAGCGACCACGATGCCAAC	94.1
	Reverse	CGAAGGTGTAGCCCTGCTCAC	
16S rRNA	Forward	AGAGTTTGATCCTGGCTCAG	93.1
	Reverse	CCGCGGCTGCTGGCAC	

Table 3. Quantitative RT-PCR sample layout on the 48 well-plate for genes Dtpsy_3433, Dtpsy_3434, Dtpsy_3435, Dtpsy_3436 and Dtpsy_3437. A similar layout was utilized for genes Dtpsy_3438, Dtpsy_1074, Dtpsy_1447 and Dtpsy_1463 on a different plate.

Fe(II) sample Dtpsy_3433	Fe(II) sample Dtpsy_3434	Fe(II) sample Dtpsy_3435	Fe(II) sample Dtpsy_3436	Fe(II) sample Dtpsy_3437	Fe(II) sample 16S rRNA
Fe(II) sample Dtpsy_3433	Fe(II) sample Dtpsy_3434	Fe(II) sample Dtpsy_3435	Fe(II) sample Dtpsy_3436	Fe(II) sample Dtpsy_3437	Fe(II) sample 16S rRNA
Fe(II) sample Dtpsy_3433	Fe(II) sample Dtpsy_3434	Fe(II) sample Dtpsy_3435	Fe(II) sample Dtpsy_3436	Fe(II) sample Dtpsy_3437	Fe(II) sample 16S rRNA
Control sample Dtpsy_3433	Control sample Dtpsy_3434	Control sample Dtpsy_3435	Control sample Dtpsy_3436	Control sample Dtpsy_3437	Control sample 16S rRNA
Control sample Dtpsy_3433	Control sample Dtpsy_3434	Control sample Dtpsy_3435	Control sample Dtpsy_3436	Control sample Dtpsy_3437	Control sample 16S rRNA
Control sample Dtpsy_3433	Control sample Dtpsy_3434	Control sample Dtpsy_3435	Control sample Dtpsy_3436	Control sample Dtpsy_3437	Control sample 16S rRNA

RESULTS

Growth curve of *Acidovorax ebreus* strain TPSY. In the Fe(III)-NTA amended control culture of strain TPSY, a maximum OD_{600} of 0.18 was reached in 10 hours with a minimal lag phase. The exponential growth phase was observed to occur between hours 2 and 8 from the start of the inoculation (Fig. 1). By contrast, in the Fe^{2+}-oxidizing strain TPSY culture, a maximum OD_{600} of 0.37 was reached after 36 hours with the first 6 hours comprising the lag phase. The exponential growth phase was observed to occur between 8 and 34 hours from the start of the inoculation (Fig. 1). In both culturing conditions, the OD_{600} began to decrease after the maximum value was reached and cells debris began to form in the culture medium. In the presence of NTA as the iron chelator, no obvious cell encrustation was observed in this study. However, iron oxide precipitates were observed along with the cell debris after the cells were lysed by sonication at the start of the protein extraction procedure.

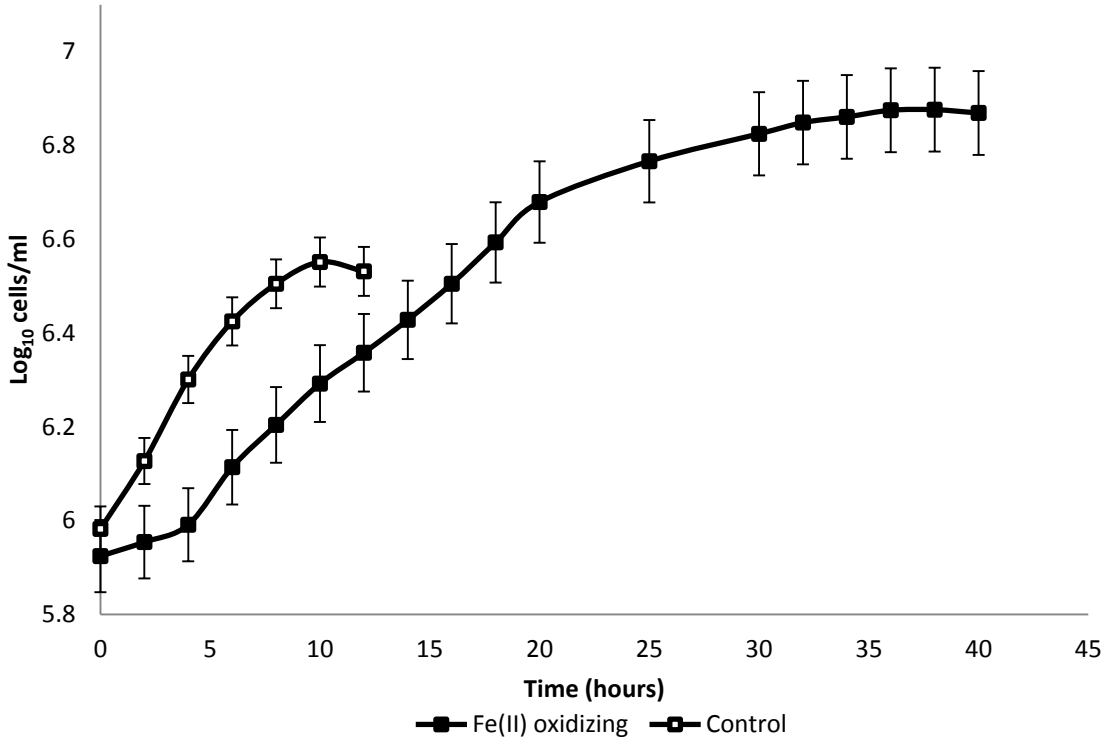

Figure 1. Growth curve of *Acidovorax ebreus* strain TPSY in iron-oxidizing environment (filled square) and control environment (open square). Cell number was calculated from the OD_{600} reading of the strain TPSY culture. The color change introduced by the formation of Fe^{3+} in the Fe^{2+}-oxidizing culture caused an negligible increment of 0.001 - 0.01 to the OD_{600} reading (<5% of the final OD_{600} reading of the Fe^{2+}-oxidizing culture).

Broad pH range 2-D electrophoretic analysis of Fe^{2+}-oxidizing and control strain TPSY protein profiles. Total protein from strain TPSY cells grown in both Fe^{2+}-oxidizing and control conditions was analyzed on broad pH range (pH 3-10) gels (Fig. 2 A and B). More than 1600 protein spots were detected on each gel from each respective condition. Most protein spots fell into the pI range of 4 to 10 with few proteins falling into a pI range of 3 to 4. Most proteins or peptides had a molecular weight between 10 to 100 kDa. The complexity of protein samples of both conditions and the resulted crowdedness of protein spots prevented accurate protein spot matching and comparison. Small pH-range 2D gels had to be utilized to fractionate protein samples before legitimate comparison could be performed. Interestingly, an extremely intense protein spot (Protein spot No. 0) which accounted for a large proportion of the whole cell protein mass was observed towards the basic end at molecular weight 37 kDa on both Fe^{2+}-oxidizing and control gels (Fig 2 A and B). According to image density calculation, this protein spot constituted a large proportion of the total protein spot density.

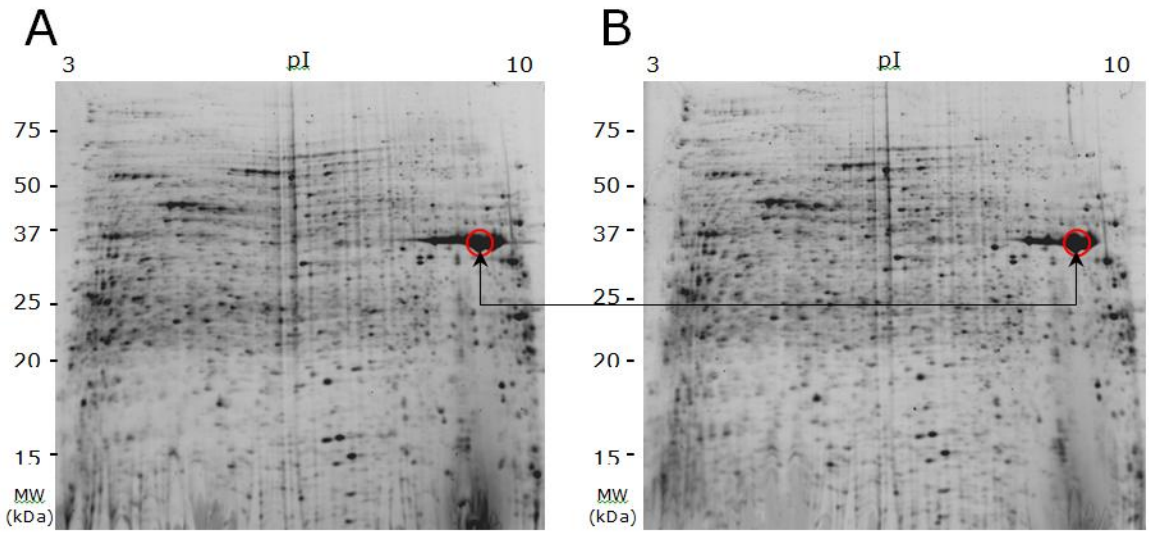

Figure 2. Broad range (pH 3-10) 2-D gel analysis of *Acidovorax ebreus* strain TPSY whole cell proteins. (A) Fe^{2+}-oxidizing cell proteins; (B) Control cell proteins. Protein spot No. 0 is indicated by the red circle.

Differentially-expressed protein recognition by small pH-range 2D gels. The application of small pH-range gels resulted in much more separated protein spots and much better overall gel resolution (Fig. 3, 4, and 5) for both Fe^{2+}-oxidizing and control protein samples. The comparison between Fe^{2+}-oxidizing and control protein gels in the acidic pH range (pH 4-7) revealed two candidate proteins that showed elevated level of expression in Fe^{2+}-oxidizing conditions compared to the control (Fig. 3). One (Protein Spot No. 1) was found near pI 6 with a molecular weight of 35 KDa (Fig. 3 A, B and C). The other (Protein Spot No. 2) was found near pI 6 and a molecular weight of 30 KDa (Fig. 3 A, B and D). The comparison in mid pH - range (pH 5-8) revealed another candidate protein that showed elevated expression in Fe^{2+}-oxidizing conditions compared to the control (Fig. 4). This protein (Protein Spot No. 3) was found near pI 5.4 with a molecular weight of 30 KDa (Fig. 4 A, B and C). Comparison of gels in the basic pH range (pH 7-10) revealed two additional candidate proteins that showed elevated expression in Fe^{2+}-oxidizing conditions compared to the control (Fig. 5). One (Protein Spot No. 4) was found near pI 8 with a molecular weight of 17 KDa (Fig. 5 A, B and C). The other (Protein Spot No. 5) was found near pI 8 with a molecular weight of 15 KDa (Fig. 5 A, B and D).

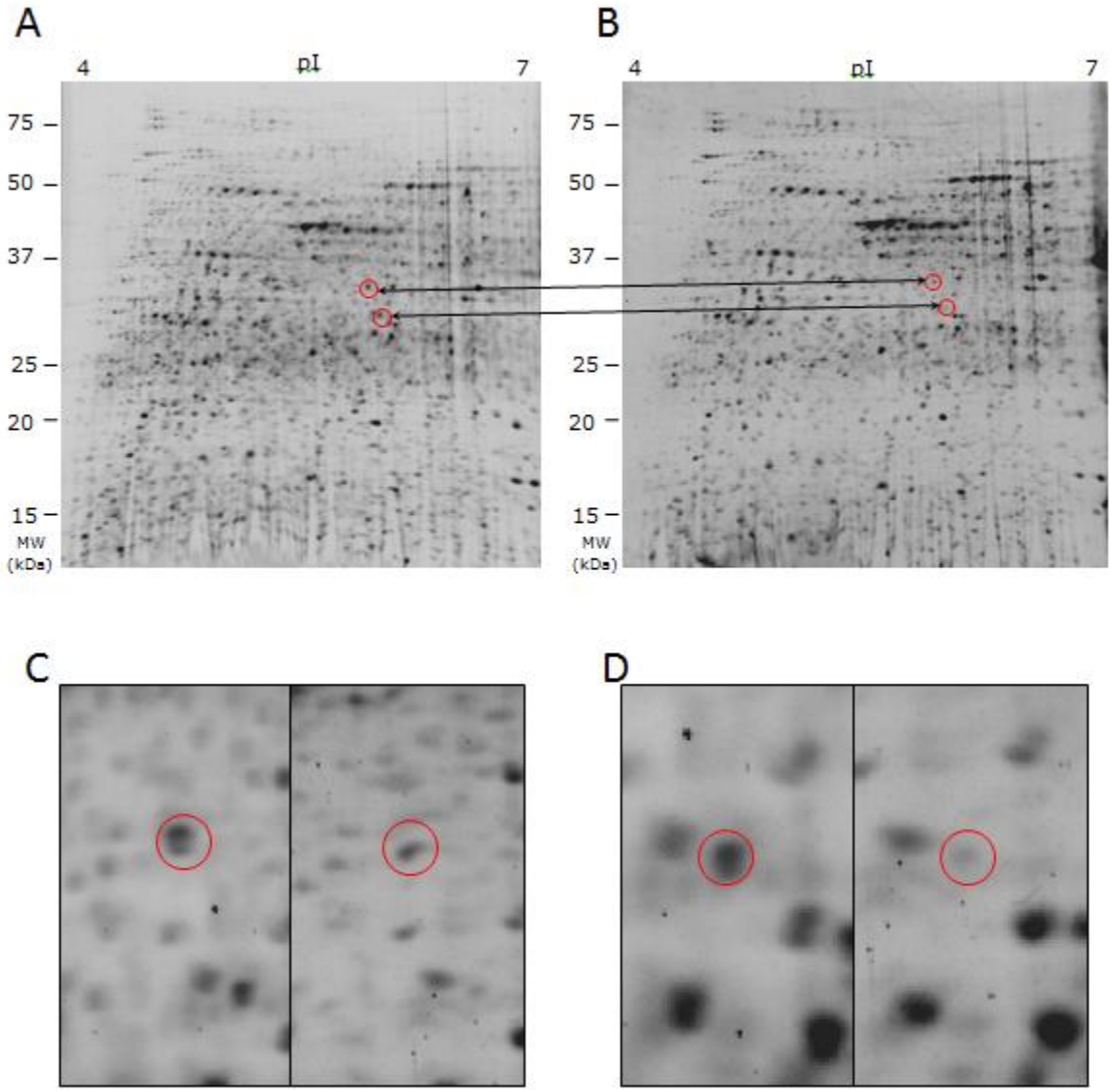

Figure 3. Acidic range (pH 4-7) 2-D gel analysis of *Acidovorax ebreus* strain TPSY whole cell proteins. (A) Fe^{2+}-oxidizing cell proteins; (B) Control cell proteins; (C) Gel comparison focused on Protein Spot No. 1 between the gels in panels A and B; (D) Gel comparison focused on Protein Spot No. 2 between the gels in panels A and B. Protein Spots No. 1 and No. 2 are indicated by the red circles.

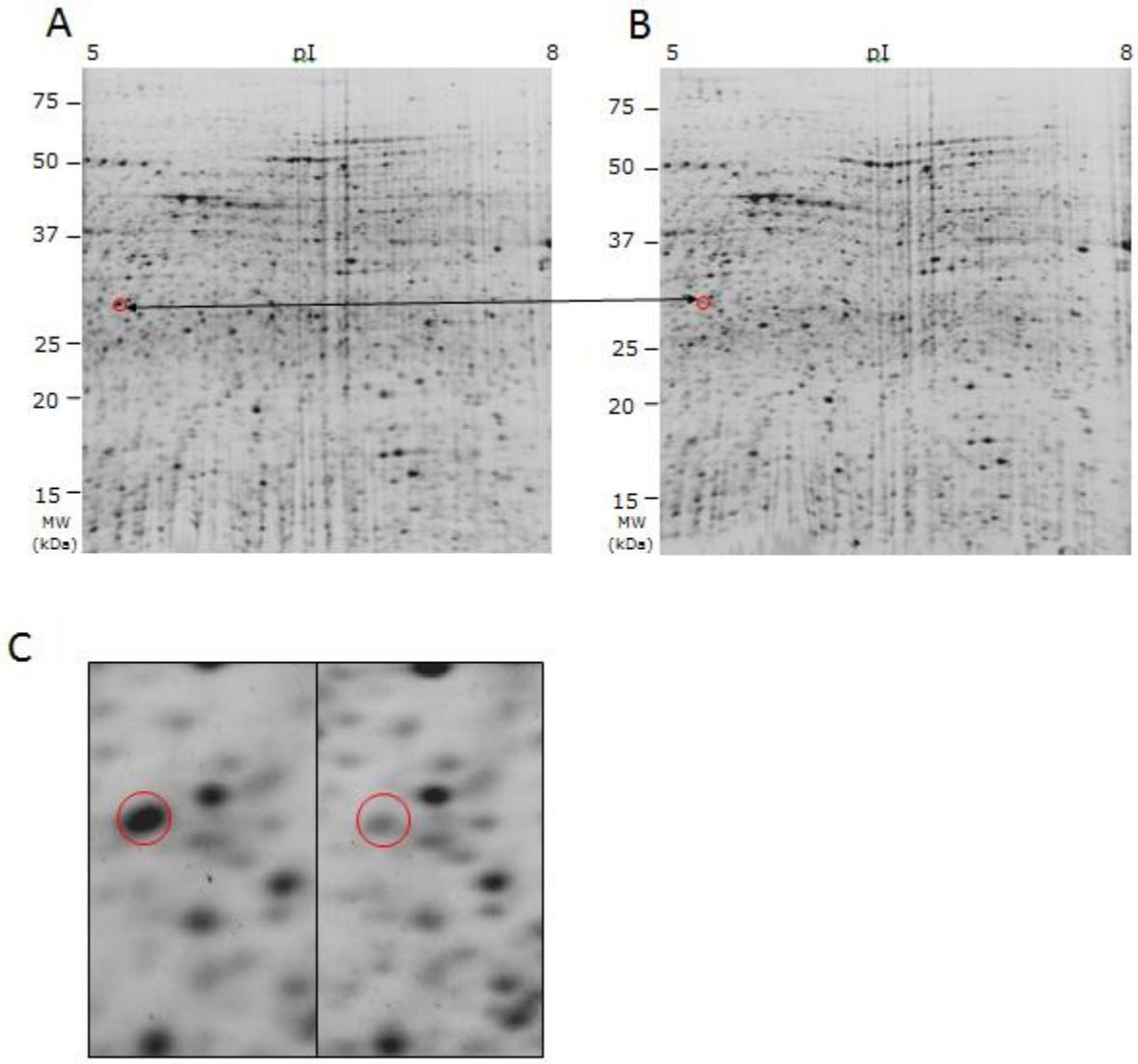

Figure 4. Small range (pH 5-8) 2-D gel analysis of *Acidovorax ebreus* strain TPSY whole cell proteins. (A) Fe^{2+}-oxidizing cell proteins; (B) Control cell proteins; (C) Gel comparison focused on Protein Spot No. 3 between the gels in panels A and B. Protein Spot No. 3 is indicated by the red circle.

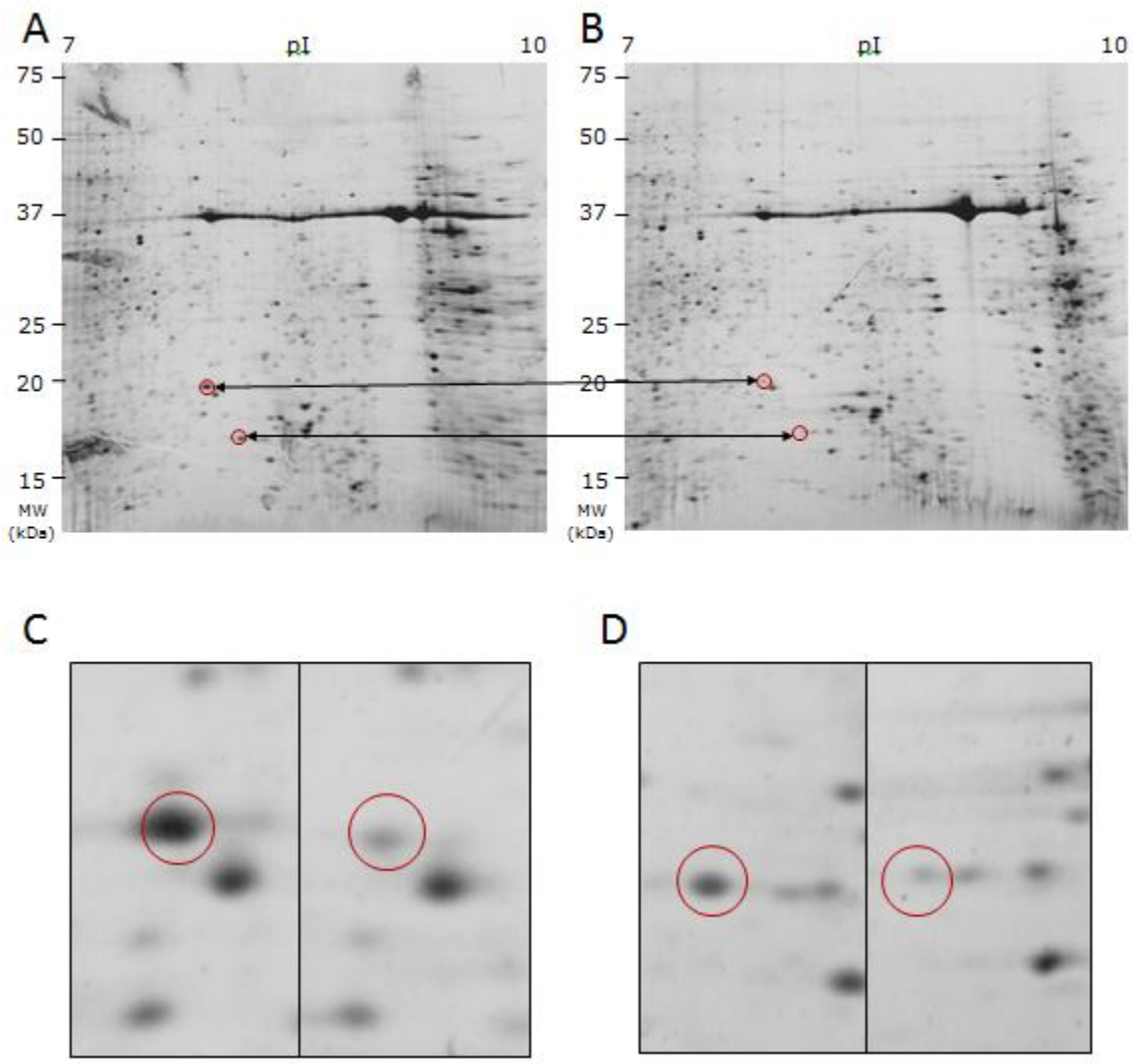

Figure 5. Basic range (pH 7-10) 2-D gel analysis of *Acidovorax ebreus* strain TPSY whole cell proteins. (A) Fe^{2+}-oxidizing cell proteins; (B) Control cell proteins; (C) Gel comparison of Protein Spot No. 4 between the gels in panels A and B; (D) Gel comparison of Protein Spot No. 5 area between the gels in panels A and B. Protein Spots No. 4 and No. 5 are indicated by red circles.

Protein identification and corresponding gene analysis. Candidate protein spots were identified by LC/MS/MS and results are shown (Table 4). Protein No. 0 was identified as a gram-negative outer membrane porin (Dtpsy_0661). Conserved domain search categorized this porin into an OM channels (outer membrane channels) superfamily. Porins in this superfamily form non-specific aqueous channels to allow the diffusion of small hydrophilic molecules across the outer membrane (11, 23, 80, 84) but they do not appear to be able to drive active transport because of the lack of energy-transducing systems (95). The Dtpsy_0661 gene and its related peripheral genes on the strain TPSY genome is displayed (Fig. 6). Conserved domain analysis of their gene products is shown in Table 5. The Dtpsy_0662 gene immediately downstream of Dtpsy_0661 encodes a gram-negative type porin which resembles Dtpsy_0661 in terms of sequence and domain function similarity. Dtpsy_0662 shares a 67% peptide sequence similarity with Dtpsy_0661. In addition, both proteins have predicted N-terminal signal peptides and belong to the same porin superfamily. Further downstream is gene Dtpsy_0663 that encodes an extracellular solute-binding protein that are mainly responsible for the uptake of a variety of substrates such as phosphate, sulfate, polysaccharides, lysine, arginine, ornithine, and histidine (37, 106).

Table 4. Identification of candidate protein spots from Fe^{2+}-oxidizing and control 2-D gels.

Protein spot No.	Accession	Protein	Protein description	Conserved domain(s)	Superfamily
0	222109877	Dtpsy_0661	Porin Gram-negative type	Gram-negative porin	OM (Outer membrane) channels
1	222110661	Dtpsy_1463	Outer membrane efflux protein, CzcC family	Not found	CzcC
2	222110645	Dtpsy_1447	Isocitrate lyase	ICL/PEPM enzyme family	ICL/PEPM_KPHMT enzyme superfamily
3	222110287	Dtpsy_1074	Alpha/beta hydrolase fold	Alpha/beta hydrolase fold	Esterase_ lipase super family
4	222112598	Dtpsy_3435	Hypothetical protein	DUF2271	DUF2271 super family
5	222112597	Dtpsy_3434	Hypothetical protein	COG5591	COG5591 super family

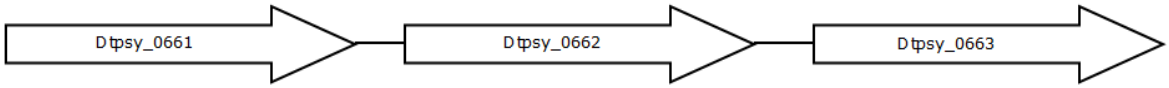

Figure 6. Schematic illustration of the Dtpsy_0661, Dtpsy_0662 and Dtpsy_0663 genes

Table 5. Conserved domain search results of the genes in the Dtpsy_0661-0663 operon.

Protein	Best BLAST hit	Conserved domain(s)	Superfamily
Dtpsy_0661	porin gram-negative type	OmpC, gram-negative porin	OM_channels
Dtpsy_0662	porin gram-negative type	OmpC, gram-negative porin	OM_channels
Dtpsy_0663	family 5 extracellular solute-binding protein	substrate-binding component of an uncharacterized ABC-type import system	PBP2, NikA, DppA, OppA like substrate binding domain

Protein No. 1 was identified as an outer membrane efflux protein (Dtpsy_1463). Notably, Dtpsy_1463 is the last one of the four genes of the Dtpsy_1460-1463 operon on the forward strand of the strain TPSY genome (Fig. 7). A conserved domain search of each encoded protein in this operon (Table 6) revealed significant similarity between this operon and the *czcCBA*-type operon that encodes a protein complex belonging to the RND (resistance, nodulation, and cell division) superfamily. Proteins in the RND superfamily are mostly involved in efflux-mediated heavy metal and drug resistance in prokaryotes (12, 50, 55, 58, 66, 76-79, 81, 90, 123, 124). Most RND proteins are encoded in operons that additionally contain the genes for a membrane fusion protein (MFP) and an outer membrane factor (OMF) (12, 58, 66, 77, 78, 81, 90), which resembles the organization of the Dtpsy_1460-1463 operon (Fig. 7 and Table 4). BLAST and conserved domain analysis revealed that Dtpsy_1460 encodes the MPF subunit (CzcB equivalent) that may serve as an adaptor protein between the RND export pump and OMF channels and play a role in RND pump activation (59, 77, 90). Dtpsy_1461 encodes the RND pump protein (CzcA equivalent), the loss of which abolishes heavy metal resistance and substrate specificity (77, 90). Although no conserved domain was directly identified in the Dtpsy_1463 gene product, it was also categorized as an outer membrane efflux protein that exhibited >80% homology with several CzcC proteins (OMF equivalents) that are involved in the formation of trans-outer membrane and trans-

periplasmic channels (77, 90). Protein Dtpsy_1462 belongs to DFU3240 (domain of unknown function). This family of proteins appears to be restricted to Proteobacteria but its function remains unclear (Conserved Domains, NCBI).

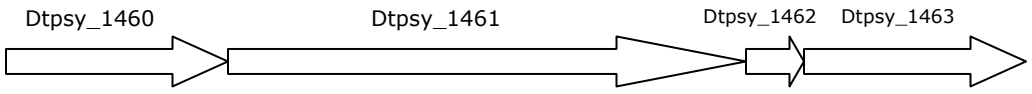

Figure 7. Schematic illustration of genes in the Dtpsy_1460-1463 operon.

Table 6. Conserved domain search results of the genes in the Dtpsy_1460-1463 operon.

Protein	Best BLAST hit	Conserved domain(s)	Superfamily
Dtpsy_1460	RND family efflux transporter MFP subunit	RND family efflux transporter, MFP subunit	RND (Resistance, nodulation, and cell division)
Dtpsy_1461	CzcA (cobalt-zinc-cadmium) family Heavy metal efflux pump	Heavy metal efflux pump CzcA subunit	CzcA
Dtpsy_1462	Putative uncharacterized protein	DUF3240	DUF3240 super family
Dtpsy_1463	Outer membrane efflux protein, CzcC family	Not found	CzcC

Protein No. 2 was identified as isocitrate lyase (Dtpsy_1447)which catalyzes the dissociation of isocitrate into succinate and glyoxylate in the first step of glyoxylate cycle. The glyoxylate cycle utilizes three of the five enzymes associated with the TCA cycle and shares many of its intermediate steps. While the TCA cycle centers on the complete oxidation of acetyl-CoA to CO_2 in order to obtain energy, the glyoxylate cycle, a carbon conserving pathway, enables the biosynthesis of carbohydrate and complex structural polysaccharides from acetyl-CoA when complex carbon sources like glucose are not available (6, 33, 51, 62, 88, 99).

Protein No. 3 was identified as an alpha/beta hydrolase fold protein (Dtpsy_1074) belonging to the under-characterized esterase_ lipase superfamily. This protein family includes structurally-related enzymes with widely differing phylogenetic origin and catalytic functions. Enzymes in this family have diverged from a common ancestor but maintain the arrangement of the catalytic residues (46, 73).

Proteins No. 4 and No. 5 were identified as hypothetical proteins belonging to the DUF2271 superfamily (Dtpsy_3435) and the COG5591 superfamily (Dtpsy_3434), respectively. Both proteins have predicted signal peptide sequences but no known predicted function. However, the genome locations of the corresponding genes of the above proteins led to an interesting discovery. The Dtpsy_3435 gene was immediately downstream of

Dtpsy_3434 gene in the Dtpsy_3433-3438 operon (Fig. 8), indicating the possibility of co-transcription of these two genes. The predicted N-terminal signal peptide and transmembrane helixes of the Dtpsy_3433 and Dtpsy_3436 gene products by InterPro (http://www.ebi.ac.uk/interpro/) indicated their membrane location. The BLAST and conserved domain search revealed that proteins encoded by genes in this operon are very likely involved in iron-related cross-membrane electron transfer (Table 7). This suggests that the Dtpsy_3433-3438 operon could be playing a critical role in anaerobic nitrate-dependent Fe^{2+} oxidation.

Dtpsy_3433 has been annotated as a ferric reductase domain-containing protein transmembrane component. Conserved domain searches revealed three conserved domains in Dtpsy_3433 (Table 7). The first one (AA 52 to AA 181) is a ferric reductase-like transmembrane domain. Blast analysis showed very broad distribution of this domain family in bacteria. This transmembrane domain is also commonly shared in mammalian cytochrome *b*-245 heavy chain (gp91-phox) and ferric reductase in yeast (Conserved domains, NCBI). The second conserved domain (AA 231 to AA 458) is a NADP-binding domain belonging to the ferredoxin-NADPH reductase (FNR) superfamily. This domain is responsible for transferring electrons from reduced ferredoxin to FAD forming $FADH_2$ via a semiquinone intermediate, followed by the transfer of two electrons and a proton to convert $NADP^+$ to NADPH (5, 15, 16, 83). The third conserved domain (AA

225 to AA 330) is an FAD-binding domain belonging to the oxidoreductase FAD-binding domain superfamily the main function of which is FAD binding and act as a prosthetic group in electron transfer like the NADPH binding domain (65). As suggested by the domain function analysis above, Dtpsy_3433 may play a role as a flavocytochrome that is capable of transferring electrons across the plasma membrane concomitant with the enzymatic transformation of iron. As expected, Dtpsy_3433 is predicted to be a ferric reductase (Conserved domains, NCBI).

A conserved domain search of periplasmic Dtpsy_3434 resulted in one conserved domain belonging to the COG5591 superfamily with no known assigned function. A conserved domain search of Dtpsy_3435 returned a similar result: a predicted periplasmic protein belonging to the DUF2271 superfamily with no known assigned function. The role of these two proteins, both of which exhibited up-regulation at the transcriptional level, remains to be elucidated.

The Dtpsy_3436 gene product has been described as an oxidoreductase Fad/NAD(P)-binding domain-containing protein harboring three conserved domains (Table 4). The first one (AA 337 to AA 467) is a flavodoxin belonging to the NADPH-dependent flavin mononucleotide (FMN) reductase superfamily. According to previous studies, flavodoxins in this family are usually found in prokaryotes and algae where they provide low potential electrons for the reduction of nitrite, $NADP^+$, and sulfite (69, 85,

109). The second conserved domain (AA 442 to AA 725) is a cytochrome P-450 reductase-like alpha subunit of SiR (sulfite reductase) belonging to the ferredoxin-NADPH reductase (FNR) superfamily. The third domain is a FAD-binding domain similar to the one possessed by Dtpsy_3433.

Dtpsy_3437 is identified as an ApbE lipoprotein (Table 4) belonging to the ApbE protein superfamily. This prokaryotic family of lipoproteins is related to ApbE from *Salmonella typhimurium* in which ApbE is involved in thiamine synthesis. More specifically, it may be involved in the conversion of aminoimidazole ribotide (AIR) to 4-amino-5-hydroxymethyl-2-methyl pyrimidine (HMP) (Conserved Domains, NCBI).

A conserved domain search of Dtpsy_3438 returned no results and a Blast search yielded few significant hits. The role of Dtpsy_3438 in anaerobic Fe^{2+} oxidation remains unknown.

Figure 8. Schematic illustration of genes in the Dtpsy_1460-1463 operon.

Table 7. Conserved domain search results of the genes in the Dtpsy_3433-3438 operon.

Protein	Best BLAST hit	Conserved domain(s)	Superfamily
Dtpsy_3433	Ferric reductase domain protein transmembrane component	(1) Ferric reductase like transmembrane domain	Ferric reductase like transmembrane domain
		(2) (NAD(P) binding domain of ferredoxin reductase-like protein	Ferredoxin reductase (FNR), an FAD and NAD(P) binding protein family
		(3) FAD-binding domain	Oxidoreductase FAD-binding domain
Dtpsy_3434	Putative uncharacterized protein	Uncharacterized conserved protein	COG5591 Superfamily
Dtpsy_3435	Putative uncharacterized protein	Predicted periplasmic protein	DUF2271 superfamily
Dtpsy_3436	Oxidoreductase FAD/NAD(P)-binding domain protein	(1) Flavodoxin	NADPH-dependent FMN reductase
		(2) Cytochrome p450- like alpha subunit of sulfite reductase	Ferredoxin reductase (FNR), FAD and NAD(P) binding protein family
		(3) FAD-binding domain	Oxidoreductase FAD-binding domain
Dtpsy_3437	ApbE family lipoprotein	ApbE family	ApbE family
Dtpsy_3438	Putative uncharacterized protein	Not found	Not found

Transcriptional level regulation analysis by Quantitative Reverse Transcription RT-PCR. Quantitative reverse transcription PCR was performed on Dtpsy_1074, Dtpsy_1447, Dtpsy_1460 and all six genes in the Dtpsy_3433-3438 operon. The relative expression level of each gene is shown in Figure 9. The Dtpsy_1463 gene showed negligible differential expression at the transcriptional level in Fe^{2+}-oxidizing conditions (96% relative to control) by qRT-PCR analysis. Genes Dtpsy_1074 and Dtpsy_1447 even showed down-regulation (26% and 18% relative to control, respectively). On the other hand, all six genes in the Dtpsy_3433-3438 operon exhibited elevated expression compared to the control. Dtpsy_3438 exhibited a 36-fold up-regulation compared to the non-iron oxidizing control, the highest expression difference among all the genes tested. Dtpsy_3433, Dtpsy_3434, Dtpsy_3435, Dtpsy_3436 and Dtpsy_3437 exhibited 12-fold, 14-fold, 23-fold, 12-fold, and 9-fold up-regulation, respectively. The up-regulation of all of the genes in this operon under Fe^{2+}-oxidizing conditions provided strong evidence that the products of this operon are of vital importance to anaerobic Fe^{2+} oxidation.

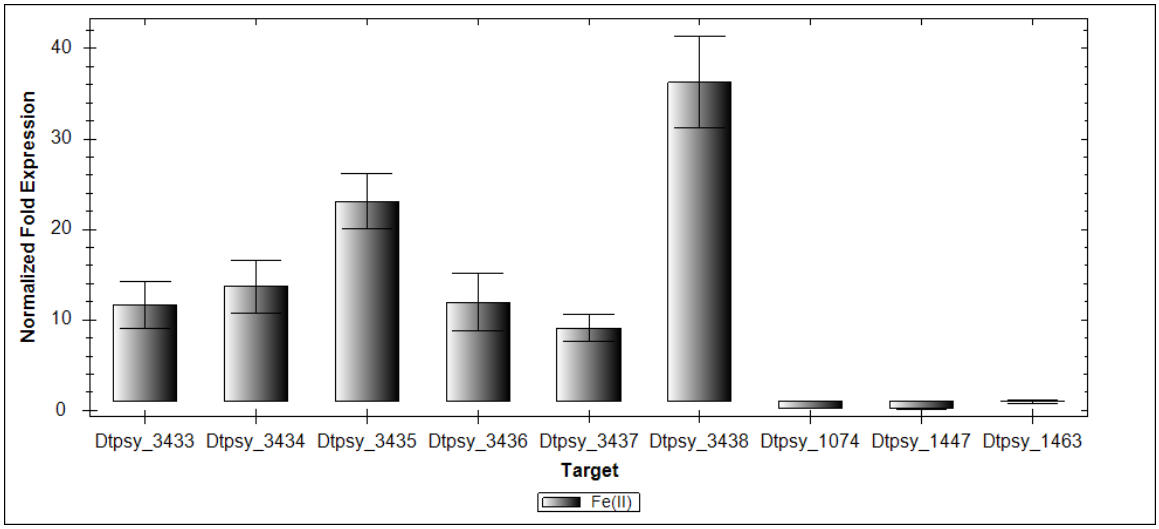

Figure 9. Quantitative reverse transcription RT-PCR analysis of the expression rate of genes of interest in Fe^{2+}-oxidizing strain TPSY cells. The expression rate of genes in the control sample was arbitrarily set to 1. Normalized fold expression change of genes in Fe^{2+} samples were all relative to control. Error bars indicate the standard deviation.

DISCUSSION

Fe(II) as additional electron donor. The presence of Fe^{2+} as an additional electron donor apparently supported the growth of the iron-oxidizing culture to more than double the cell density of the control culture with acetate as the sole electron donor. Similar results were obtained by Coates *et al.* when strain TPSY was cultured autotrophically and mixotrophically (117). This confirmed the fact that Fe^{2+} is a preferred electron donor over acetate. The presence of Fe^{2+} prevented acetate from being used as an electron donor so comparatively more acetate was used as the carbon source as a result. Also, Fe^{2+} oxidation coupled to nitrate reduction provided additional energy needed for the much more robust growth of strain TPSY in the Fe^{2+}-oxidizing culture. The lag phase of the Fe^{2+}-oxidizing strain TPSY culture could be simply explained by the synthesis of RNA, enzymes and other molecules required for this metabolism since initial inoculation was made by the transfer of an active anaerobic strain TPSY culture pre-grown on nitrate (12 mM) and acetate (6.25 mM) without any ferrous iron amendment. The absence of a significant lag phase in the control culture also indicated that Fe^{3+} reduction, if any in the presence of nitrate, exerted little impact on the culture growth as described earlier. Despite its obvious effect on the growth of the strain TPSY culture, iron amendment at the concentration of 2 mM exerted no significant toxicity effect. A recent report using up to 9 mM EDTA-chelated Fe(II) as an

amendment in the growth study of *Acidovorax delafieldii* 2AN did not result in obvious physiological toxicity response (17), suggesting the high iron-tolerance ability of the *Acidovorax* genus.

Periplasmic precipitation of iron oxide. The cellular location of anaerobic nitrate-dependent Fe(II) oxidation has long been debated. It is commonly recognized that the enzymatic transformation of Fe(II) to Fe(III) takes place on the outer membrane or in the periplasm as supported by the outer membrane localization of potential key enzymes involved in this metabolism (34, 64, 114, 120). This is also supported by the outer cellular and periplasmic encrustation by iron oxide during the growth of anaerobic nitrate-dependent Fe(II) oxidizers in the absence of an iron-chelating agent (49, 52, 70, 71). Particularly, in the study of iron oxide encrustation of *Acidovorax* sp. strain BoFeN1, it was found that the precipitation started rapidly in the periplasm, then progressed to the surface of the cell (70), indicating the periplasmic location of the enzymatic transformation of Fe(II) to Fe(III) and the resultant formation of iron oxide. This is also likely the case in our study because iron oxide precipitation was only observed after the disruption of the cell structure. It is likely that it is the equilibrium between the periplasmic formation of iron oxide and the outer cellular chelator-mediated solubilization that makes possible the continuous Fe(II) oxidation across the outer membrane.

Dtpsy_0661-0663 gene cluster analysis. The domain function analysis

of the Dtpsy_0661-0663 gene cluster suggests that the Dtpsy_0661 gene and its neighboring gene cluster are mainly involved in the passive transport of small nutrition molecules across the outer membrane. In addition, Dtpsy_0661 protein was nearly equally expressed in both Fe^{2+}-oxidizing and control cells; thus, it is believed to be involved in the cross membrane diffusion of small nutrition molecules rather than iron-specific transport. To our knowledge, this is the first report using solid 2D gel electrophoresis evidence that such a large proportion of the whole cell protein mass from any gram-negative bacterium is accounted for by a gram-negative porin protein.

Dtpsy_1460-1463 operon analysis. The reason for the elevated expression of the Dtpsy_1460-1463 efflux protein complex is intriguing. Since iron, an essential nutrient for bacteria, is not usually considered toxic at ambient concentration, there has been no report of iron detoxification by an RND family-efflux pump. However, the periplasmic accumulation of high concentrations of Fe^{3+} from the oxidation of Fe^{2+} could pose a serious threat to bacteria (4, 14, 19, 41, 74, 76, 82, 86, 108, 113, 119) and trigger the functioning of the RND family efflux pump system. This hypothesis is coincident with previous discussions on the membrane protein-mediated transformation of Fe^{2+} to Fe^{3+} and the resulting periplasmic accumulation of Fe^{3+}. Although qRT-PCR failed to prove the transcriptional up-regulation of the Dtpsy_1460-1463 operon, given the proteomic analysis it is likely that

the operon is regulated at the translational level or through post-translational modification.

Dtpsy_1447 analysis. As a key enzyme in the carbon-conserving glyoxylate cycle, the up-regulated isocitrate lyase (Dtpsy_3437) in Fe^{2+}-oxidizing cells could indicate a much more active production of structural carbohydrates. A possible explanation could be drawn this way: contrary to the Fe^{2+}-absent control medium, the presence of Fe^{2+} as an additional electron donor frees the acetate of being both the electron donor and the carbon source, thus yielding more available acetate to be used for organic cell material synthesis. This explanation is coincident with the more robust growth of Fe^{2+}-oxidizing strain TPSY cultures compared to the control. Despite the reasonable explanation of the translational up-regulation of isocitrate lyase in Fe^{2+}-oxidizing conditions, the detailed regulatory mechanism of this gene remains to be investigated.

Dtpsy_3433 analysis. The functional and structural similarity of Dtpsy_3433, yeast ferric reductase, and cytochrome *b*-245 heavy chain makes possible several hypothetical enzymatic activities of Dtpsy_3433 (Fig. 10). This commonly shared domain configuration is characterized by an N-terminal transmembrane iron-related enzymatic module and a C-terminal electron transfer-related module containing FAD/NADP binding domain. Previous studies indicated that cytochrome *b*-245 is a flavocytochrome, the first described in higher eukaryotic cells, bearing the complete electron-

transporting apparatus of the NADPH oxidase (98). Its low-potential heavy chain (gp91-phox) is reported to be a flavin adenine dinucleotide (FAD)-dependent dehydrogenase and NADPH oxidoreductase with electron transferase activity that reduces molecular oxygen to superoxide anions as a side reaction (94, 98). Mutations in the heavy chain (gp91-phox) lead to the X-linked chronic granulomatous disease which is characterized by the absence of a functional plasma membrane-associated NADPH oxidase (1, 26, 30, 63, 93, 94, 98, 107). The electron transferase activity of the gp91-phox heavy chain is supported by further studies that demonstrate it is the heme-binding subunit of cytochrome *b*-245 (27, 68, 121, 122). Furthermore, studies from the Dtpsy_3433 homolog in yeast have shown that Frp1 and Fre1, the ferric reductase transmembrane component from *S. pombe* and *S. cerevisiae*, respectively, are required for both cell surface ferric reductase activity and ferric iron uptake (3, 28, 29, 38, 91). Thus, it is reasonable to believe that this domain of Dtpsy_3433 is playing a role in electron transfer coupled to enzymatic iron transformation on the membrane. The notably reversibility of ferredoxin-NADP reductase catalyzed reactions (5, 15, 16, 47) and its significant chemical resemblance to the Fe-S system of the bacterial electron transfer chains that reduce cytochrome P-450 (8, 45, 47, 92) lead to the following hypothesized role of Dtpsy_3433 in Fe^{2+} oxidation. Coupled with the nitrate/nitrite reduction system, the predicted ferric reductase may

perform the reverse reaction of ferric reduction: conducting electron transfer from ferrous iron to nitrate through cytochrome P-450-like intermediates.

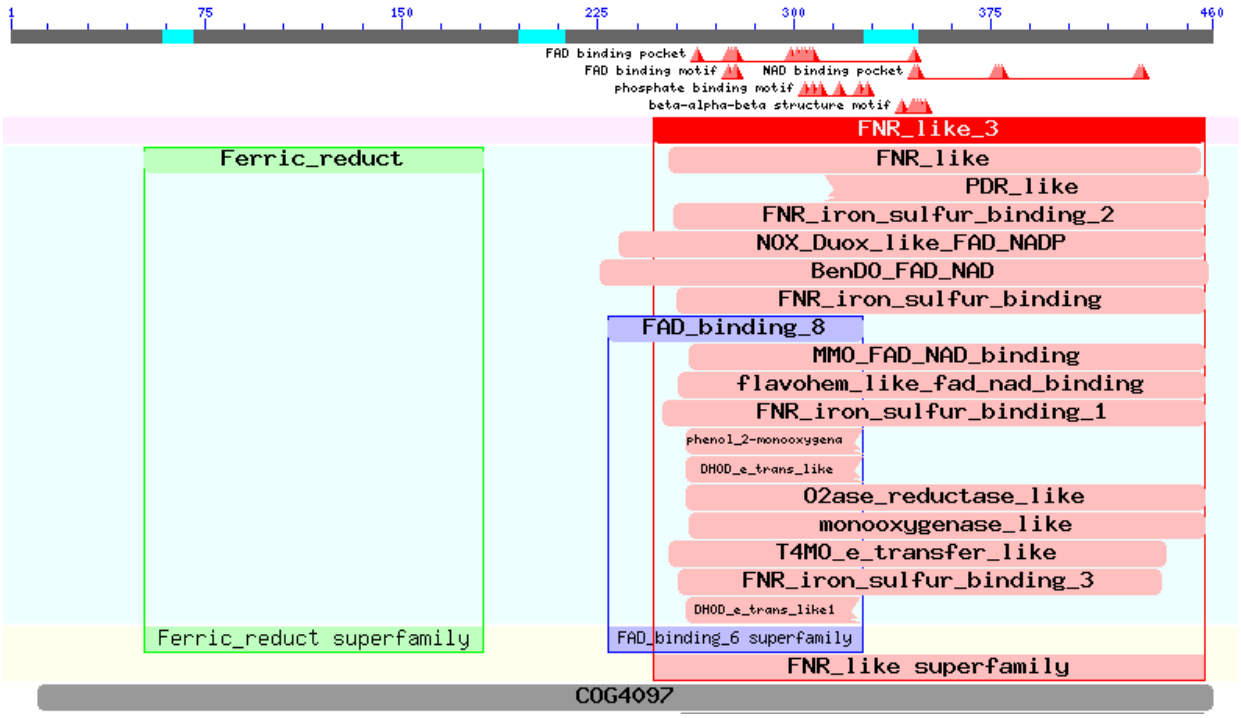

Figure 10. Illustration of a common domain configuration in Dtpsy_3433, yeast ferric reductase, and cytochrome *b*-245 heavy chain. (Adapted from Conserved Domain, NCBI)

Dtpsy_3436 analysis. Besides an N-terminal transmembrane domain of unknown function, Dtpsy_3436 possesses a C-terminal domain configuration homologous to sulfite reductase in *E.coli* and cytochrome *P*-450 reductase (Fig. 11). Previous studies of SiR (sulfite reductase) in *E. coli* revealed that this multimeric hemoflavoprotein is composed of eight electron-donating alpha subunits and four catalytic hemoprotein beta subunits. Each alpha subunit binds one FAD and one FMN as prosthetic groups and contains an NADPH domain. The electron transfer starts from NADPH to FAD, FMN and finally to the metal center of the beta subunit where the reduction of sulfite takes place (39, 47). Reduction of nitrite by plant sulfite reductase, which showed significant sequence homology to NADPH-SiR of *E. coli*, has also been observed, demonstrating the broad substrate diversity of this enzyme family (24, 72). Thus, the Dtpsy_3436 gene product is apparently another important component of the electron transport chain in anaerobic Fe^{2+} oxidation. Its domain structure homology with cytochrome P-450 reductase and sulfite reductase alpha subunit indicated its potential role as an electron transfer component of the nitrite/sulfite reductase system that receives electrons from the putative ferrous iron oxidase (Dtpsy_3433) and transfers them to a cytochrome in the electron transfer chain which eventually terminates with the reduction of nitrate.

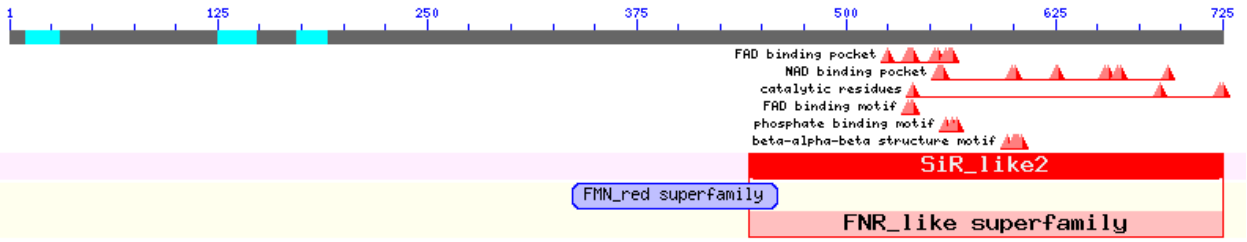

Figure 11. Illustration of domain configuration of Dtpsy_3436. (Adapted from Conserved Domain, NCBI)

Dtpsy_3437 analysis. The connection between Dtpsy_3437, an ApbE family protein, and anaerobic Fe^{2+} oxidation metabolism is very vague so far. Previous research of the ApbE protein in *Salmonella typhimurium* revealed its periplasmic location and its role in thiamine synthesis (9, 10). More recent research identified the FAD-binding motif (13) of some members of this family and their similarity to NosX protein, another member of the ApbE family, which has been implicated in nitrous oxide reduction (18). In addition, ApbE has been suggested to function in Fe-S cluster metabolism by affecting metal cofactor assembly (100, 101). The latter function is more likely the case in our study considering the co-expression of the Dtpsy_3433 and Dtpsy_3436 genes. It is therefore reasonable to predict that Dtpsy_3437 may also play a role in FAD-mediated electron transfer and the normal functioning of Fe-S protein similar to Dtpsy_3433.

A hypothesized anaerobic nitrate-dependent Fe^{2+} oxidation model. To conclude, the proteomics and qRT-PCR approach generated both direct

and indirect evidence for a series of proteins that may be critical components in the anaerobic nitrate-dependent Fe^{2+} oxidation pathway in *Acidovorax ebreus* strain TPSY. A predicted model of the role of each identified component is presented (Fig. 12). Briefly, small nutrition molecules such as Fe^{2+} and nitrate enter the periplasm through passive diffusion. Fe^{2+} is oxidized by the Dtpsy_3433 ferric reductase using a reverse mechanism and transfers electron to the ferredoxin component of Dtpsy_3433. The electron is then transferred to Dtpsy_3436 through intermediate quinones like FAD, FMN, and NADP. The electron is further transferred to cytochromes, and finally to the nitrate/nitrite reduction system where denitrification occurs, completing the cycle. Accumulated Fe^{3+} in the periplasm is exported to the extracellular space by the Dtpsy_1460, Dtpsy_1461 and Dtpsy_1463 outer membrane efflux protein complex, preventing the accumulation of periplasmic iron oxide.

This study serves as an initial attempt to investigate the anaerobic nitrate-dependent oxidation of Fe^{2+} at the molecular level. The results of the current work will provide insight for further research into the identification of other pathway components and will lead to a more comprehensive understanding of the molecular genetics of this metabolism.

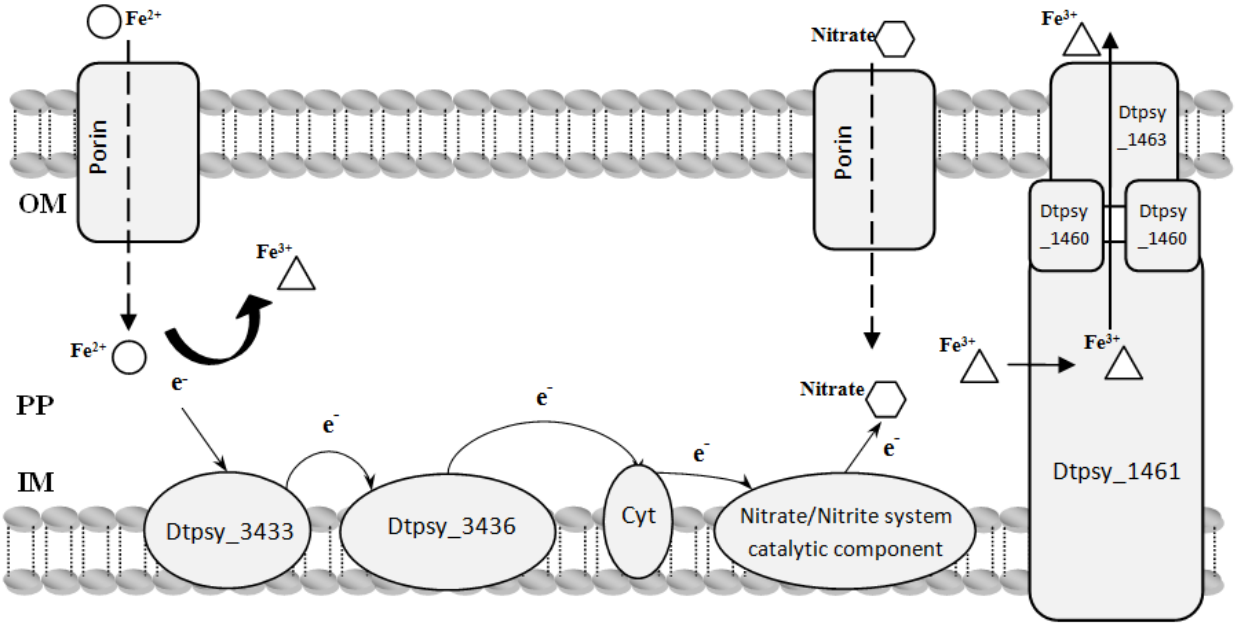

Figure 12. Schematic illustration of the putative roles of proteins involved in anaerobic nitrate dependent Fe^{2+} oxidation. Electron flow is described in detail in the text. OM, outer membrane. PP, periplasm. IM, inner membrane. Cyt, cytochrome.

SECTION 2

ABSTRACT

Perchlorate is a wide-spread contaminant detected in drinking water and ground water systems in the United States. The current development of a highly sensitive enzymatic bioassay for *in situ* perchlorate concentration quantification created a need for high-quality and low-cost perchlorate reductase.

Perchlorate reductase, originally isolated from DPRB (dissimilatory perchlorate reducing bacteria), is encoded by an operon containing four genes, *pcrABCD*. Enzymatically active perchlorate reductase purified by traditional methods is composed of two structural subunits, PcrA and PcrB, encoded by the *pcrA* and *pcrB* genes, respectively. The lengthy traditional protein purification process and the slow growth rate of DPRB hinder the industrial mass production of this enzyme.

In this study, we report an attempt to use *E. coli* host to overexpress perchlorate reductase and use a polyhistidine tag to enable ease of the subsequent purification. The *pcrAB* genes encoding the structural subunits of perchlorate reductase were cloned into an expression vector in *E. coli.* The purification of the recombinant perchlorate reductase was performed under strict anaerobic and denaturing conditions and a highly purified form of the

enzyme was obtained. Possible solutions to avoid the formation of inclusion bodies while still maintaining the enzyme activity were discussed. This work proved the feasibility of recombinant perchlorate reductase expression using an *E.coli* host and the usefulness of the histidine tag in the purification process.

In addition, this work provided insights into factors that need to be taken into future consideration in order to obtain the recombinant enzyme with full enzymatic activity. As a final goal, this study will contribute to the development of enzyme-based bioassay for the detection of perchlorate in the environment by lowering the production and purification cost of its key component, the perchlorate reductase.

INTRODUCTION

Toxicity and regulation of perchlorate. Perchlorate (ClO_4^-), a compound commonly used in automobile airbags, seat belt pre-tensioner and solid rocket fuel, is a wide-spread environmental contaminant that has been detected in both drinking water and groundwater systems in the United States (9, 15, 39). Perchlorate poses a serious health threat due to its interference with iodine uptake into the thyroid gland (2, 9, 14, 22, 35, 40). As a result, the U.S. Environmental Protection Agency (EPA) issued a recommended Drinking Water Equivalent Level (DWEL) and a "Cleanup Guidance" for perchlorate of 24.5 µg/L in early 2006. On February 11, 2011, the EPA issued a "regulatory determination" that perchlorate meets the Safe Drinking Water Act criteria for regulation as a contaminant, which began a process to determine what level of contamination is appropriate for regulation (http://www.regulations.gov/#!documentDetail;D=EPA-HQ-OW-2008-0692-2369). Due to the strict requirement of sophisticated instruments and specialized personnel for the current mass spectrometry-based perchlorate detection method (19), a more cost-effective enzyme activity-based detection method with higher sensitivity is being pursued (32) (16) and a bioassay system allowing the detection in the parts per billion (ppb) range has been achieved (16).

Microbial remediation of perchlorate by dissimilatory perchlorate-

reducing bacteria (DPRB). Despite the increasing concern over perchlorate contamination, the current strategy for the remediation of perchlorate mostly relies on microbially mediated biodegradation due to the chemical stability of perchlorate in the environment and its high solubility in water (24, 38). It has been known for some time that specialized microorganisms could couple anaerobic growth to the reduction of chlorate or perchlorate and completely reduce them to innocuous chloride with simple organic or inorganic electron donors (1, 6, 7, 12, 20, 25, 26, 31, 33, 42, 43). These organisms are phylogenetically diverse with members belonging to the α-, β-, γ-, and ε-subclass of the *Proteobacteria* (9, 12, 20, 29). The majority are in the β-*Proteobacteria* and are members of the genus *Dechloromonas* or *Dechlorosoma* (1, 12). A recent report of the discovery of a gram-positive thermophilic bacterium, *Moorella perchloratireducens* sp. nov., capable of perchlorate reduction (3) shows the broad distribution of perchlorate reduction metabolism among prokaryotes. Physiological studies have demonstrated that many of the known DPRB possess a broad range of metabolic capacities including the oxidation of hydrogen (28), simple organic molecules (6, 12), aromatic hydrocarbons (10), reduced humic substances (10, 11), ferrous iron (6, 7, 12, 20), and hydrogen sulfide (6, 12).

The perchlorate reduction pathway. The DPRB mediated perchlorate reduction pathway consists of two central enzymes: perchlorate reductase and chlorite dismutase. Illustrated bellow (Fig. 1), perchlorate reductase

reduces perchlorate to chlorite in the first step of the pathway. The formed chlorite is subsequently converted to chloride and water in the presence of reductive force (5, 9).

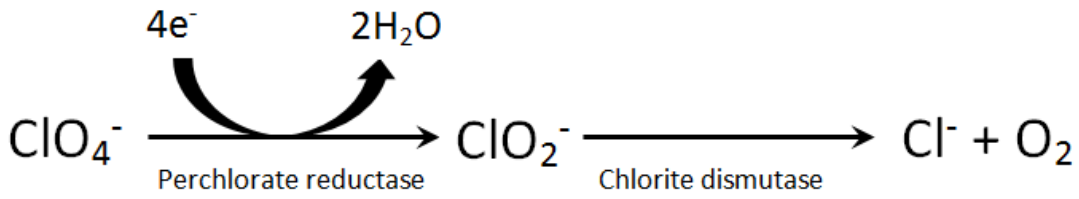

Figure 1. Illustration of the perchlorate reduction pathway of DPRB.

Perchlorate reductase. Perchlorate reductase, originally identified in dissimilatory perchlorate-reducing bacteria (DPRB), is encoded by operon *pcrABCD*. This operon encodes two structural subunits (PcrA and PcrB), a cytochrome (PcrC), and a molybdenum chaperone subunit (PcrD). The structural PcrA subunit is an electron transfer protein of approximately 96 kDa possessing a pterin molybdenum cofactor and iron-sulfur centers. The other structural subunit PcrB is a polypeptide of approximately 40 kDa that has four cysteine-rich clusters for Fe-S center binding which are likely responsible for electron transfer to the molybdopterin-containing PcrA subunit. The PcrC subunit is a *c*-type cytochrome of approximately 25 kDa responsible for connecting the reductase to the membrane. The PcrD subunit is thought to be a system-specific molybdenum chaperone protein of approximately 25 kDa (5). Recent research revealed that functional

perchlorate reductase purified by traditional methods is only composed of the two structural subunits, PcrA and PcrB. The PcrC subunit is believed to be lost during the purification of the enzyme with no affect on enzyme activity. The PcrD subunit is believed to be involved in the assembly of the mature perchlorate reductase prior to periplasmic translocation but not to be part of the active enzyme (18, 30).

Significance of this study. The traditional perchlorate reductase purification procedure is not cost-effective for industrial application for several reasons: the extremely slow growth rate of most DPRB (6, 8, 12), the complicated environmental factors that influence the induction of the enzyme (5, 8), and the lengthy purification procedure that requires highly specialized instruments and technicians (18, 30). Thus, a more cost-effective and less time-consuming perchlorate reductase expression and purification scheme is needed. In this study, we report the heterologous over-expression of perchlorate reductase in *E. coli* and the usefulness of a histidine-tag in the process of purification.

MATERIALS AND METHODS

Genomic DNA extraction. Genomic DNA extraction was conducted using the DNeasy Blood & Tissue Kit (QIAGEN). In brief, *Dechloromonas aromatica* RCB cells were harvested from a 1.5-ml overnight culture by centrifugation at 7,500×g for 5 min. Cell pellets were resuspended in 180 µl Buffer ATL. Cells were lysed by the addition of 20 µl proteinase K and incubated at 56°C for 10-20 min. Occasional vortexing was performed during incubation to disperse the sample. After the complete lysis of the cells, the lysate sample was vortexed for 15 s. Buffer AL (200 µl) was added to the sample and mixed thoroughly by vortexing. Ethanol (96–100%, 200 µl) was then added and the mixture was vortexed. The sample mixture was transferred using a pipet into the DNeasy Mini Spin Column placed in a 2-ml Collection Tube and centrifuged at 6000 x g for 1 min. The flow-through and collection tube were discarded. Then the DNeasy Mini Spin Column was place in a new 2-ml Collection Tube. Buffer AW1 (500 µl) was added to the column and centrifuged at 6000 x g for 1 min. The flow-through and collection tube were discarded. The DNeasy Mini Spin Column was placed in a new 2-ml collection tube. Buffer AW2 (500 µl) was added and centrifuged at 12,000 x g for 3 min to dry the DNeasy membrane. The flow-through and collection tube were discarded. The DNeasy Mini Spin Column was place in a clean 2-ml microcentrifuge tube and Buffer AE (200 µl) was pipetted directly onto the DNeasy membrane. After an incubation at room temperature for 1 min,

genomic DNA was eluted by centrifugation at 6000 x g for 1 min.

PCR amplification. PCR amplification was performed using the *Pfx50* DNA Polymerase PCR system (Invitrogen). Primers (Table 1) were synthesized by Integrated DNA Technologies. A 50-µl PCR reaction containing 5 µl *Pfx50* PCR Mix (10X), 1.5 µl dNTP Mix (10 mM), 2 µl primer mix (10 µM each), 1 µl *Dechloromonas aromatica* RCB genomic DNA, 1 µl *Pfx50* DNA Polymerase, and 38.5 µl double-distilled water was subjected to the following PCR protocol: initial denaturation at 94^{o}C for 5 min followed by 35 cycles of denaturation at 94^{o}C for 30 seconds, annealing at 60^{o}C for 1 min and extension at 72^{o}C for 1 min, followed by a final extension at 72^{o}C for 5 min. The PCR product was analyzed by agarose gel (0.7%) electrophoresis.

Table 1. Primers used in PCR.

Primer	Sequence
pAB forward	CACCATGGTTCAAATGACACGAAGA
pAB reverse	GGTCAAAGGAGAAATCATCAT
pBAD-Reverse	GATTTAATCTGTATCAGG
Txn-Forward	TTCCTCGACGCTAACCTG

Expression vector construction and transformation. The successfully amplified PCR product was inserted into the expression vector pBAD202/D-TOPO (Invitrogen) according to the instructions provided. In brief, the cloning reaction (6 µl) containing fresh PCR product (2 µl), Salt Solution (1 µl), sterile water (2 µl), and TOPO vector (1 µl) was prepared in a

microcentrifuge tube, mixed gently using a pipet and incubated in room temperature for 5 min. The reaction was stored on ice after the incubation. The cloning reaction (3 µl) was added into a vial of One Shot TOP10 Chemically Competent *E. coli* cells (Invitrogen), mixed gently and incubated on ice for 20 min. The cells were heat-shocked at 42^{o}C for 30 seconds without shaking and the tube was immediately transferred onto ice. Room-temperature S.O.C. medium (250 µL, Invitrogen) was added to the tube. The tube was tightly capped and shaken horizontally at 200 RPM at 37^{o}C for 1 hour. Transformed cells (100 µL) were spread on a pre-warmed LB + kanamycin (25 µg/ml) plate and incubated overnight at 37^{o}C.

Plasmid preparation. Plasmid preparation was performed using the Plasmid Mini Prep kit (QIAGEN). In brief, *E. coli* colonies harboring the expression plasmid vector with the *pcrAB* insert (named plasmid pAB) were picked, grown overnight in LB + kanamycin, and 1 ml of the culture was harvested in a microcentrifuge tube by centrifugation at 12,000 × g for 1 min. Cell pellets were resuspended in Buffer P1 (250 µl). Buffer P2 (250 µl) was added to the tube and mixed thoroughly by inverting the tube 4–6 times to lyse the cells. Then Buffer N3 (350 µl) was added and mixed immediately by inverting the tube 4–6 times. The tube was centrifuged for 12,000 × g for 10 min to pellet the proteins and genomic DNA. The supernatant was transferred to the QIAprep spin column by pipetting. The column was centrifuged at 12,000 × g for 30–60 s and the flow-through was discarded.

The QIAprep spin column was washed by adding Buffer PB (0.5 ml) and centrifuged at 12,000 × g for 30–60 s. The flow-through was discarded. The QIAprep spin column was washed again by adding Buffer PE (0.75 ml) and centrifuged at 12,000 ×g for 30–60 s. After the flow-through was discarded, the column was centrifuged at 12,000 × g for an additional 1 min to remove residual wash buffer. The QIAprep column was then placed in a clean 1.5 ml microcentrifuge tube. Buffer EB (50 µl) was added directly to the center of the spin column. The column was allowed to stand for 1 min and centrifuged at 12,000 × g for 1 min to elute the plasmid DNA.

Restriction enzyme digest. Restriction enzymes used in this study were purchased from Promega and restriction digests were performed according to the manufacturer's instructions. In brief, a reaction of 20 µl containing plasmid DNA (1 µl), restriction enzyme (1 µl), 10× buffer (2 µl), and nuclease-free water (16 µl) was incubated at 37^{o}C for 1 hour in a heat block followed by heat-inactivation at 65^{o}C for 15 min. The digestion products were analyzed by agarose gel electrophoresis.

Cell cultivation and recombinant protein expression induction. Manipulation of the anaerobic cell cultures was conducted in an anaerobic hood unless otherwise specified. LB + kanamycin (25 µg/ml) medium (50 ml) in a 250-ml flask was inoculated with 0.5 ml of an overnight *E.coli* culture transformed with pAB and was incubated at 37^{o}C in an anaerobic candle jar. An anaerobic environment was achieved using a H_2-CO_2 gas pack (BD BBL

Anaerobic System). Arabinose from a sterile anaerobic stock solution was added to the culture at early log phase (OD_{600}=0.5) to a final concentration of 0.2% to induce the expression of the *pcrAB* genes. After incubation for 6 hours, the 50-ml culture was transferred to a 50-ml centrifuge tube and cells were collected by centrifugation at 7,500 × g for 15 min.

Purification. All reagents used in the anaerobic purification process were prepared under anoxic conditions and all the purification procedures were performed in an anaerobic glove box unless otherwise specified. The recombinant protein purification was performed using the Ni-NTA Purification System (Invitrogen). In brief, the Ni-NTA column was prepared using the following protocol: Ni-NTA resin (2 ml) was poured into a 10-ml Purification Column, the resin was allowed to settle completely by gravity for 15 min after which the resin was resuspended in sterile distilled water (6 ml). After the supernatant was discarded, the resin was resuspended in Denaturing Binding Buffer (6 ml) and allowed to settle; the supernatant was discarded. The harvested cell pellets with the expressed recombinant protein were resuspended in Guanidinium Lysis Buffer (8 ml) with Sarkosyl (0.2%) and incubated on a rocking platform for 10 min to ensure thorough cell lysis. The cell lysate was sonicated on ice with ten 10-second pulses at medium intensity. The lysate was centrifuged at 12,000 × g for 20 min to pellet the cellular debris. The supernatant was loaded onto the previously prepared Ni-NTA column. The column was incubated at room temperature with gentle

agitation for 30 minutes. The resin was allowed to settle and the supernatant was stored at 4^{o}C. Then the resin was washed twice with Denaturing Binding Buffer (4 ml) for 2 min and allowed to settle. The supernatant was stored at 4^{o}C. The resin was washed three additional times with the following buffers in order: Denaturing Wash Buffer with 1 mM Sodium Dithionite (pH 6.0, 4 ml), Denaturing Wash Buffer with 1 mM Sodium Dithionite (pH 5.3, 4 ml) and Denaturing Wash Buffer with 1 mM Sodium Dithionite (pH 4.0, 4 ml). The supernatant from the above three wash steps were individually stored at 4^{o}C until use.

Protein sample preparation and SDS-PAGE. SDS-PAGE was performed using the mini PROTEAN protein electrophoresis system (Bio-Rad). Protein samples collected from each purification step were subjected to TCA (trichloroacetic acid) precipitation. In brief, one volume of cold TCA was added to 4 volumes of protein sample in a microcentrifuge tube and incubated on ice for 10 min. The tube was centrifuged at 12,000 × g for 5 min to pellet the proteins and the supernatant was discarded. The protein pellet was washed twice with cold acetone (200 µl). Protein pellets were collected at the bottom of the tube by centrifugation at 12,000 × g for 5 min. The tube was then placed in a 95^{o}C heat block for 5 min to dry the pellets. After the completion of the TCA precipitation, the protein pellets were resuspended in SDS loading buffer (63 mM Tris HCl, 10% glycerol, 2% SDS, 0.0025% bromophenol blue, pH 6.8, 5-10 µl). Then the sample was heated

in a boiling water bath for 5 min and loaded onto an 11% hand-casted PAGE gel. Electrophoresis was performed at 200V constant for 50 min. The gel was rinsed in water for 5 min three times before staining with SimplyBlue SafeStain (Invitrogen) for 1-2 hours.

Western blot. Electrophoretic transfer was performed using the Mini Trans-Blot electrophoretic transfer cell (Bio-Rad). In brief, the SDS-PAGE gel was rinsed in transfer buffer (25 mM Tris, pH 8.3, 192 mM glycine, 20% methanol, 0.1% SDS). A piece of nitrocellulose membrane (Bio-Rad) cut to the size of the gel was soaked in transfer buffer for 2 min and then rinsed in deionized water for 2 min. The gel transfer sandwich was assembled in a gel holder cassette with the following items in order (from bottom to top): one pre-wetted fiber pad on the grey side of the cassette, a sheet of filter paper (Whatman) cut to the size of the gel, the equilibrated gel, pre-wetted membrane, a piece of filter paper, and another pre-wetted fiber pad. A glass roller was used to gently roll out any air bubbles that formed between the sandwich layers. The cassette was closed firmly and inserted into the module. The module and the frozen blue cooling unit were placed in the tank which was then filled with transfer buffer. A stir bar was added to the tank to maintain even buffer temperature. The transfer was carried out at 200 V constant for 2 hours at 4^{o}C. Upon the completion of the electrophoretic transfer, the membrane was blocked in 1 × TBST buffer (2.5 mM Tris, 15 mM NaCl, 0.005% Tween 20) with 5% non-fat milk at room temperature for

1 hour. The membrane was then incubated in 10,000-fold diluted primary antibody (rabbit-anti-PCR IgG) for 1 hour. The membrane was washed with TBST buffer for 10 min three times and then incubated in 25,000-fold diluted secondary antibody (anti-rabbit IgG attached to horseradish peroxidase) at room temperature for 2 hours. The membrane was washed with TBST for 10 min three more times and then presented to substrate for 5 minutes. Film development was performed using an autodeveloper.

RESULTS

Expression vector confirmation. The construction of the expression vector pAB is illustrated in Fig. 2. Restriction enzyme (Sma I) digest confirmed the size of the vector with the insert to be 8.2 kb (Fig. 3, lane 1, lane 2). The correct location and orientation of the insert were further validated by a cross-primers PCR method. PCR was performed using a pcrAB Forward primer and a pBAD-Reverse primer and again using a Txn-Forward primer and a pcrAB Reverse primer which generated PCR products of 3.8 kb and 3.9 kb in size, respectively (Fig. 3, lane 4, lane 7), which is in accordance with the insertion orientation as illustrated (Fig. 2).

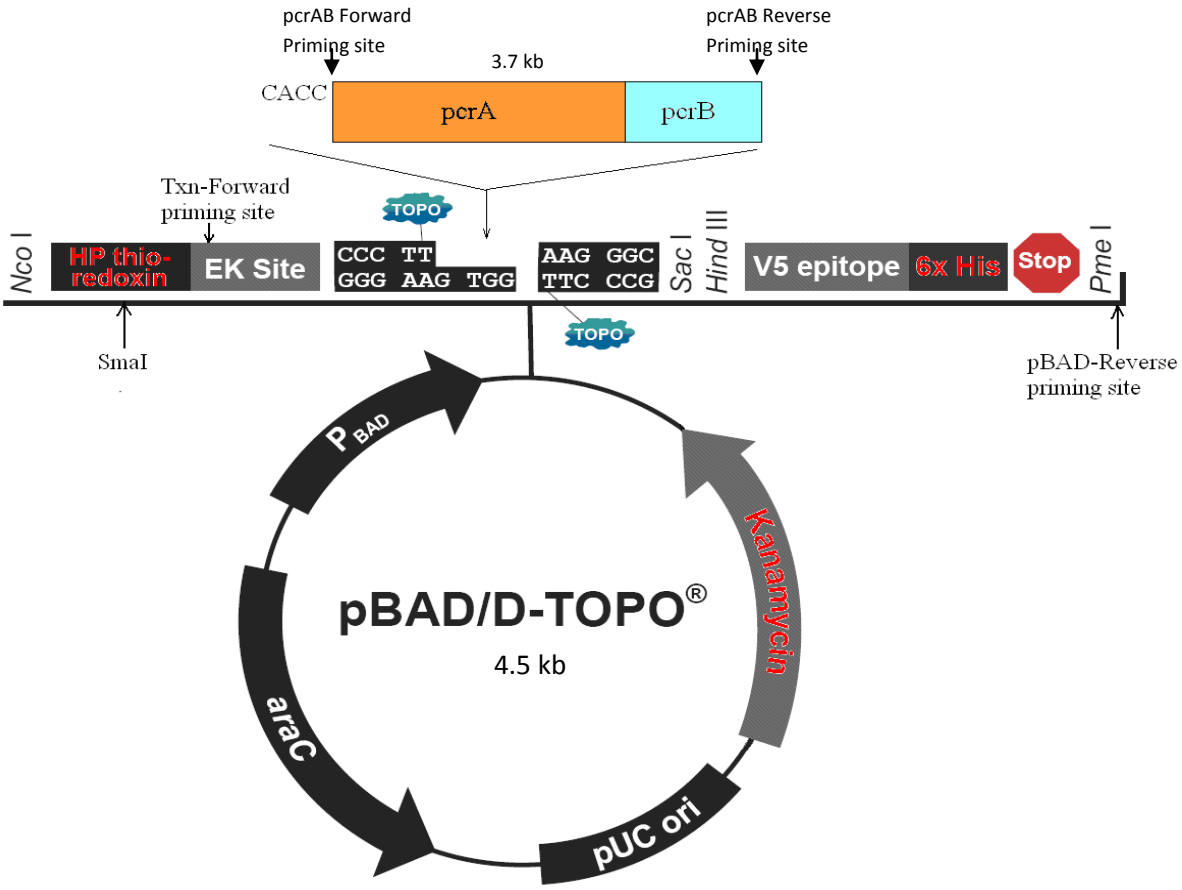

Figure 2. Expression vector pBAD-pcrAB. SmaI cutting site and priming sites of primers used in cross-primer PCR are indicated by arrows. (Adapted from product manual, Invitrogen)

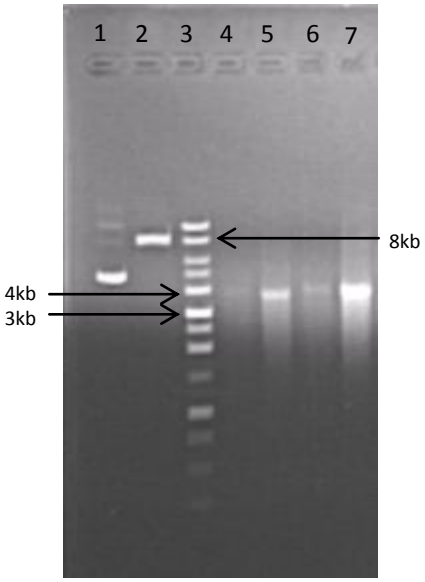

Figure 3. Agarose gel analysis of SmaI-digested pAB and its cross-primer PCR products. Lane 1, pAB; lane 2, pAB digested by Sma I; lane 3, 10 kb size marker; lane 4, PCR primer pair: pcrAB Forward + pBAD Reverse; lane 5, PCR primer pair: pcrAB Forward + pcrAB Reverse; lane 6, PCR primer pair: Txn Forward + pBAD Reverse; lane 7, PCR primer pair: Txn Forward + pcrAB Reverse.

Target protein expression and confirmation. The SDS-PAGE analysis of *E.coli* cells expressing the recombinant PcrAB showed the successful expression of both PcrA and PcrB subunits (Fig. 4, lane 5) when compared to the untransformed and uninduced controls (Fig. 4, lane 1 and lane 2). The N-terminal thioredoxin fusion protein added 13 kDa to the PcrA subunit and made final size of the Thio-PcrA 109 kDa, which appeared as a band at the top of the gel (Fig. 4, lane 5). The 6 × histidine tag added 5 kDa to the expressed PcrB subunit and made the final size of PcrB-His 45 kDa, which appeared as a thin band in the middle of the gel (Fig. 4, Lane 5).

Western blot analysis verified the identity of the expressed proteins (Fig. 5). The band signals of Thio-PcrA (109 kDa) and PcrB-His (45 kDa) proteins (Fig. 5, lane 3) were clearly identified by comparing to untransformed and uninduced controls (Fig. 5, lane 1, lane 2). A few non-specific band signals were also observed (Fig. 5, lane 3). This could be caused by the quality of the antibody since similar band signals were also observed in the controls (Fig. 5, lane 1 and lane 2).

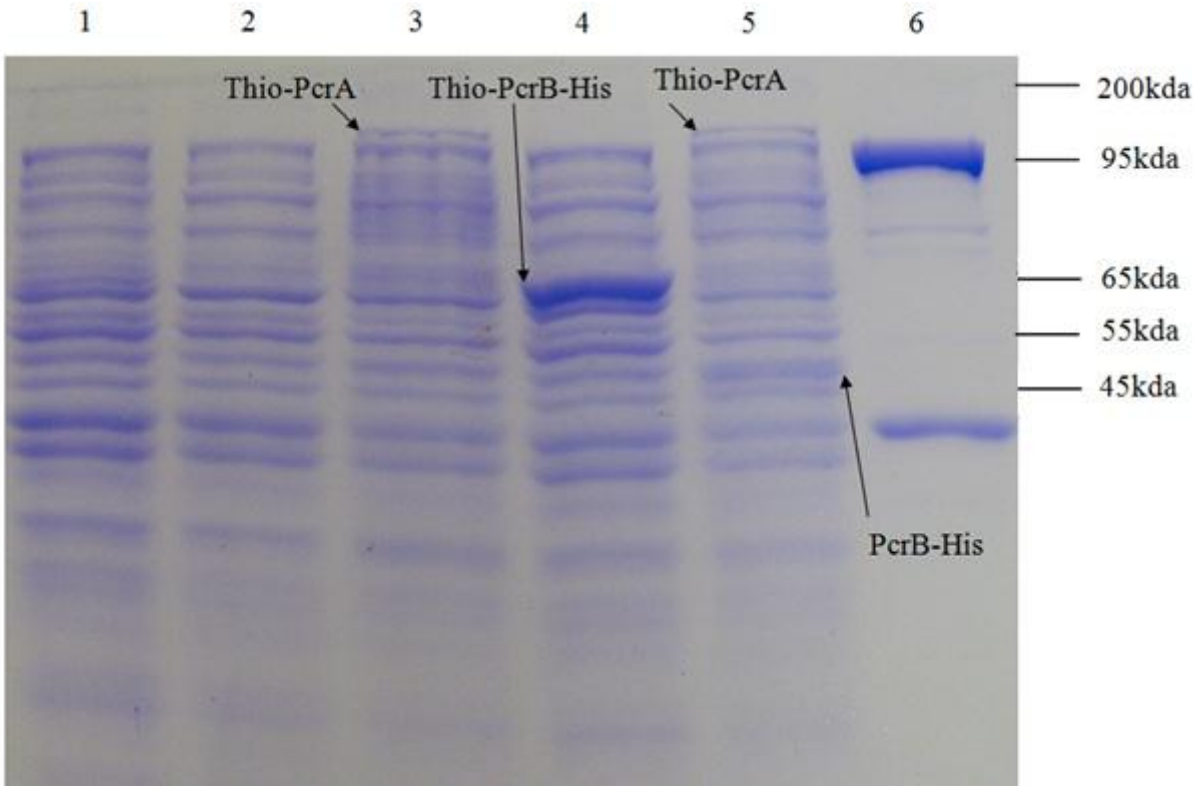

Figure 4. SDS-PAGE analysis of the expression of recombinant PcrAB protein. Lane 1, plasmid free *E. coli* cells; lane 2, uninduced pAB harboring *E. coli* cells; lane 3, *E. coli* cells expressing recombinant PcrA; lane 4, *E. coli* cells expressing recombinant PcrB; lane 5, *E. coli* cells expressing PcrAB; lane 6, native perchlorate reductase PcrAB from *D. aromatica* RCB.

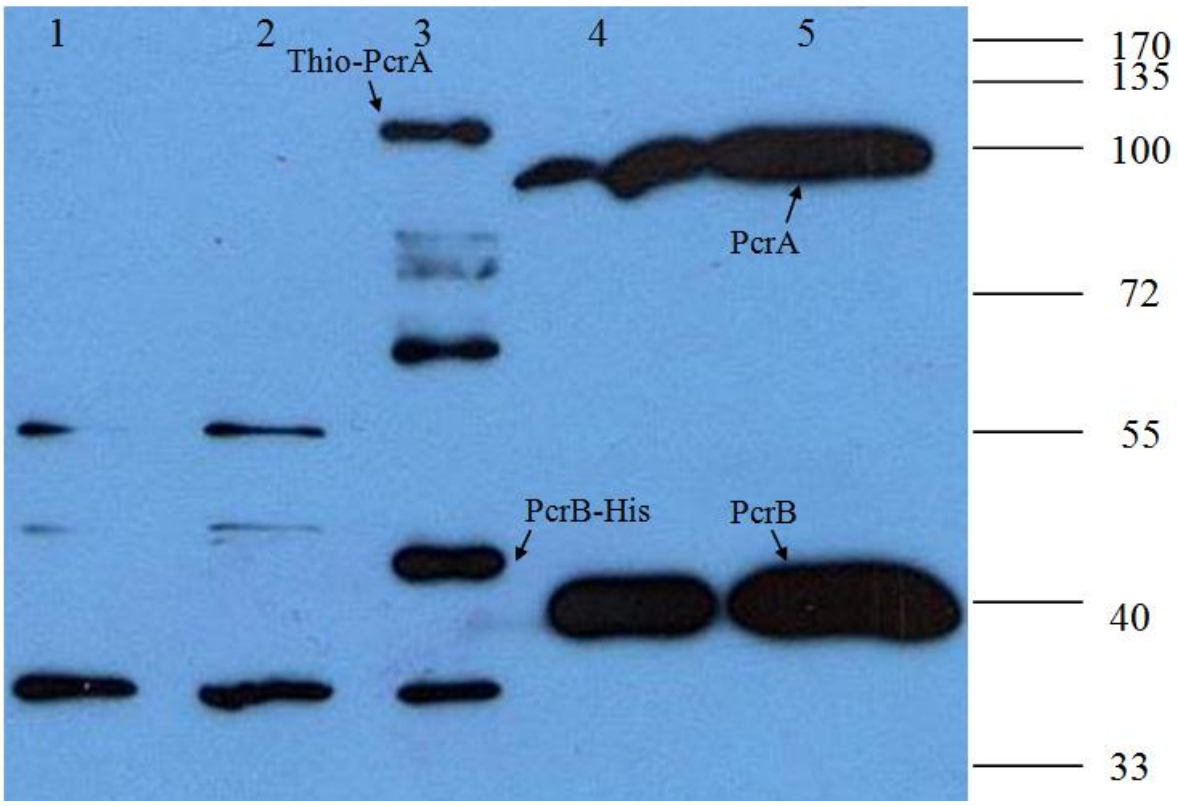

Figure 5. Western blot analysis of *E.coli* cells expressing recombinant PcrAB protein. Lane 1, plasmid free *E.coli*; lane 2, *E.coli* cells harboring pAB, uninduced; lane 3, *E.coli* cells expressing PcrAB; lane 4 and lane 5, perchlorate reductase PcrAB from *D. aromatica* RCB.

Purification of the recombinant proteins. Our initial attempt to purify PcrAB under native conditions was not successful because the expressed recombinant PcrAB accumulated in insoluble inclusion bodies. Thus, guanidine lysis buffer-based denaturing conditions were utilized with sarkosyl as an inclusion body solubilizer. The SDS-PAGE results showed the co-purification of PcrA and PcrB subunits (Fig. 6). When the pH of the wash buffer was decreased to 6.0, a small amount of PcrA and PcrB began to elute from the column (Fig. 6, lane 7). When the pH of the wash buffer was further decreased to 5.3, most of the resin-bound PcrA and PcrB was eluted with little contamination from other proteins (Fig. 6, lane 8). The remaining PcrA and PcrB were eluted when the pH was decreased to 4.0 (Fig. 6. Lane 9). The pH 5.3 and pH 4.0 eluent fractions were combined. The purified PcrAB sample was sent to Dr. Coates's lab in University of California at Berkeley to be dialyzed and refolded. However, the sample after the renaturation process did not show any enzymatic activity.

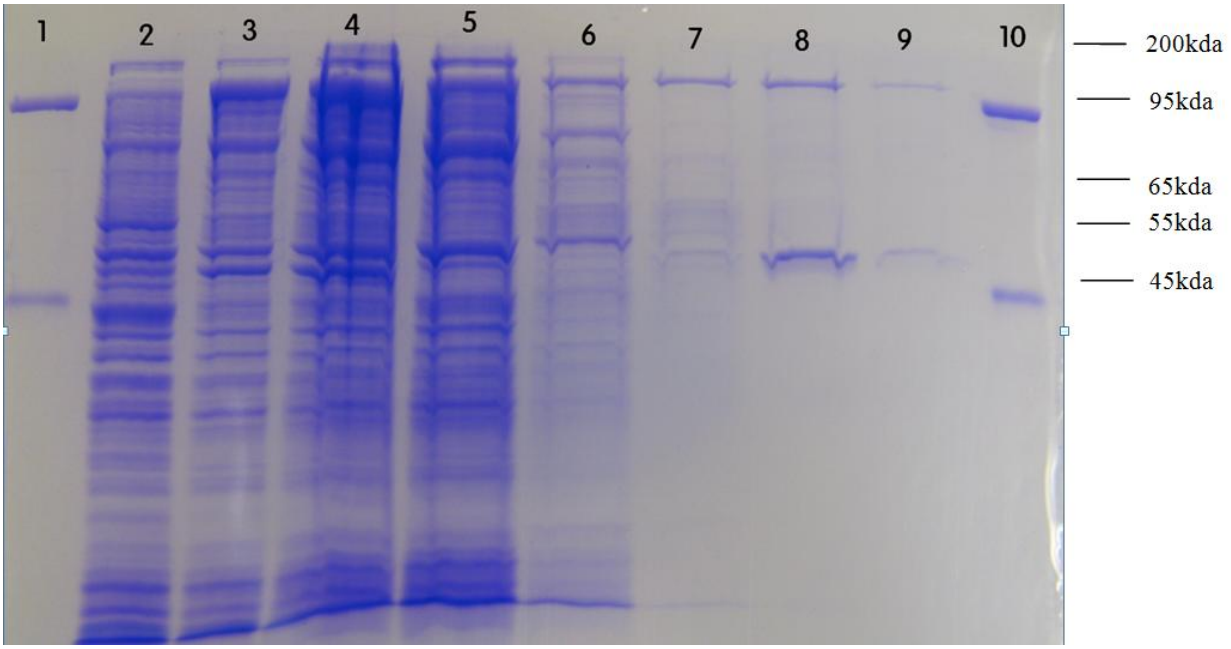

Figure 6. SDS-PAGE analysis of the purification of recombinant PcrAB protein. Lane 1, lane 10, perchlorate reductase from *Dechloromonas RCB*; lane 2, pAB harboring *E. coli* lysate, uninduced, control; lane 3, pAB harboring *E. coli* lysate, induced; lane 4, pAB harboring *E. coli* lysate supernatant; lane 5, flow-through supernatant after binding with column; lane 6, column wash through, pH 7.8; lane 7, column wash through, pH 6.0; lane 8, column wash through, pH 5.3; lane 9, column wash through, pH 4.0.

DISCUSSION

Location of the 6 × histidine tag on the recombinant enzyme. To determine the proper location of the 6 × histidine tag, structural information about the PcrAB complex was required. This was mostly obtained from examining nitrate reductase, a close relative of perchlorate reductase in the type II DMSO reductase family (5, 27). The nitrate reductase encoded by the *narGHIJ* operon shares significant functional subunit similarity with the perchlorate reductase, with NarG and NarH being the structural subunits, NarI being the cytochrome and NarJ being the chaperone (41). Previous crystal structural studies of nitrate reductase revealed that the C-terminal of the NarH subunit is free of any space inhibition in NarGH complex (17). Considering that the PcrAB complex could employ a similar structure, the 6 x histidine tag sequence was added downstream of *pcrAB* so that the 6 x histidine tag would be fused to the C-terminal of the recombinant PcrB.

The thioredoxin fusion protein. The thioredoxin sequence on the pBAD plasmid was added upstream of the *pAB* gene to express the thioredoxin as a fusion protein tag to the recombinant PcrAB protein since this fusion tag has previously been shown to improve the expression rate and solubility of foreign proteins (21). However, the thioredoxin fusion protein did not help with the solubility of PcrAB in this study.

Expression optimization. A series of procedures were performed to avoid the formation of inclusion bodies and increase the solubility of the expressed

protein. The use of sarkosyl at a low concentration as an inclusion body solubilizer was previously reported to be able to maintain the native activity of the heterologously expressed actin in *E. coli* (13). However, sarkosyl (0.2%) in native lysis conditions did not result in the solubilization of the formed inclusion bodies.

Previous research reported that the co-expression of chaperone proteins helped the folding and the solubility of heterologous recombinant proteins (23). However, the attempt to amplify and clone the entire perchlorate reductase operon *pcrABCD* did not succeed. The reason might be that the size of the *pcrABCD* (5.3kb) operon exceeded the appropriate accommodation threshold of the pBAD vector. An alternative was to express PcrD in another expression plasmid with a different antibiotic selective marker. The additional cost of antibiotic would compromise the initial goal as to increase the production rate while lowering the cost of this enzyme.

The third attempt made was adding NO_3^- (10 mM) to the culture medium to induce the expression of nitrate reductase and see if the nitrate reductase chaperon NarJ, the homolog of perchlorate reductase chaperone PcrD, could help with the folding and solubility of PcrAB. However, this approach did not yield a detectable amount of soluble PcrAB.

The approach of lowering the induction temperature (30^{o}C, 24^{o}C and 16^{o}C) combined with a lower concentration of inducing agent (0.02% and 0.002% arabinose) did not yield soluble PcrAB.

Other expression optimization approaches to be considered. One solution could be switching to a different *E.coli* strain. Different *E.coli* strains tend to have different genetic responses to foreign recombinant proteins and different cytoplasmic protein expression environment like pH and redox state, which may favor the expression of some recombinant proteins while disfavor the others (34, 37). The second solution may still lie in the co-expression of perchlorate chaperone proteins. Co-expression of chaperone proteins has long been shown to be an important factor of the correct folding for heterologous recombinant proteins, thus preventing the insolubility of misfolded proteins and the formation of inclusion bodies (4, 36). Due to the large size of the perchlorate reductase gene operon, the construction of an expression vector accommodating the entire *pcrABCD* operon becomes an obstacle. An expression vector that is able to accept a large size insertion-sequence will be needed for effective cloning and transformation.

Importance of this study. Although the purified PcrAB protein did not possess enzyme activity, this work demonstrated the feasibility of using an *E.coli* host to express perchlorate reductase and the effectiveness of using a histidine-tag in the purification process. This purification methodology could also be applied to similar proteins in the type II DMSO family. In addition, this work provided an experimental platform on which further expression optimization could be performed in order to obtain soluble perchlorate reductase with full enzymatic activity.

REFERENCE

Section 1

1. **Abo, A., A. Boyhan, I. West, A. J. Thrasher, and A. W. Segal.** 1992. Reconstitution of neutrophil NADPH oxidase activity in the cell-free system by four components: p67-phox, p47-phox, p21rac1, and cytochrome *b*-245. J. Biol. Chem. **267:**16767-16770.
2. **Achenbach, L. A., U. Michaelidou, R. A. Bruce, J. Fryman, and J. D. Coates.** 2001. *Dechloromonas agitata* gen. nov., sp. nov. and *Dechlorosoma suillum* gen. nov., sp. nov., two novel environmentally dominant (per)chlorate-reducing bacteria and their phylogenetic position. Int. J. Syst. Evol. Microbiol. **51:**527-533.
3. **Anderson, G. J., E. Lesuisse, A. Dancis, D. G. Roman, P. Labbe, and R. D. Klausner.** 1992. Ferric iron reduction and iron assimilation in *Saccharomyces cerevisiae*. J. Inorg. Biochem. **47:**249-255.
4. **Andrews, S. C., A. K. Robinson, and F. Rodriguez-Quinones.** 2003. Bacterial iron homeostasis. FEMS Microbiol. Rev. **27:**215-237.
5. **Arakaki, A. K., E. A. Ceccarelli, and N. Carrillo.** 1997. Plant-type ferredoxin-NADP+ reductases: a basal structural framework and a multiplicity of functions. FASEB J. **11:**133-140.

6. **Ashworth, J. M., and H. L. Kornberg.** 1963. Fine control of the glyoxylate cycle by allosteric inhibition of isocitrate lyase. Biochim. Biophys. Acta. **73:**519-522.

7. **Barnett, M. O., P. M. Jardine, and S. C. Brooks.** 2002. U(VI) adsorption to heterogeneous subsurface media: application of a surface complexation model. Environ. Sci. Technol. **36:**937-942.

8. **Batie, C. J., and H. Kamin.** 1984. Electron transfer by ferredoxin:NADP+ reductase. J. Biol. Chem. **259:**11976-11985.

9. **Beck, B. J., and D. M. Downs.** 1998. The *apbE* gene encodes a lipoprotein involved in thiamine synthesis in *Salmonella typhimurium*. J. Bacteriol. **180:**885-891.

10. **Beck, B. J., and D. M. Downs.** 1999. A periplasmic location is essential for the role of the ApbE lipoprotein in thiamine synthesis in *Salmonella typhimurium*. J. Bacteriol. **181:**7285-7290.

11. **Benz, R.** 1988. Structure and function of porins from gram-negative bacteria. Ann. Rev. Microbiol. **42:**359-393.

12. **Blair, J. M., and L. J. Piddock.** 2009. Structure, function and inhibition of RND efflux pumps in Gram-negative bacteria: an update. Curr. Opin. Microbiol. **12:**512-519.

13. **Boyd, J. M., J. A. Endrizzi, T. L. Hamilton, M. R. Christopherson, D. W. Mulder, D. M. Downs, and J. W. Peters.** FAD binding by ApbE

protein from *Salmonella enterica*: a new class of FAD-binding proteins. J. Bacteriol. **193:**887-895.

14. **Braun, V.** 1997. Avoidance of iron toxicity through regulation of bacterial iron transport. Biol. Chem. **378:**779-786.

15. **Carrillo, N., and E. A. Ceccarelli.** 2003. Open questions in ferredoxin-NADP+ reductase catalytic mechanism. Eur. J. Biochem. **270:**1900-1915.

16. **Ceccarelli, E. A., A. K. Arakaki, N. Cortez, and N. Carrillo.** 2004. Functional plasticity and catalytic efficiency in plant and bacterial ferredoxin-NADP(H) reductases. Biochim. Biophys. Acta. **1698:**155-165.

17. **Chakraborty, A., J. Schieber, and F. W. Picardal.** 2011. Influence of nitrate-dependent, Fe(II) oxidation on growth of *Acidovorax delafieldii* 2AN: a comparative approach. Presented at the 111th General Meeting of the American Society for Microbiology, New Orleans, LA, May 20th - May 24th.

18. **Chan, Y. K., W. A. McCormick, and R. J. Watson.** 1997. A new *nos* gene downstream from *nosDFY* is essential for dissimilatory reduction of nitrous oxide by *Rhizobium (Sinorhizobium) meliloti*. Microbiology **143:**2817-2824.

19. **Chiancone, E., P. Ceci, A. Ilari, F. Ribacchi, and S. Stefanini.** 2004. Iron and proteins for iron storage and detoxification. Biometals **17:**197-202.

20. **Coates, J. D., and R. T. Anderson.** 2000. Emerging techniques for anaerobic bioremediation of contaminated environments. Trends Biotechnol. **18:**408-412.

21. **Coates, J. D., R. Chakraborty, J. G. Lack, S. M. O'Connor, K. A. Cole, K. S. Bender, and L. A. Achenbach.** 2001. Anaerobic benzene oxidation coupled to nitrate reduction in pure culture by two strains of *Dechloromonas*. Nature **411:**1039-1043.

22. **Cornell, R. M., and U. Schwertmann.** 2003. The Iron Oxides: Structure, Properties, Reactions, Occurrences, and Uses. 2nd ed. Wiley-VCH, Weinheim.

23. **Cowan, S. W., T. Schirmer, G. Rummel, M. Steiert, R. Ghosh, R. A. Pauptit, J. N. Jansonius, and J. P. Rosenbusch.** 1992. Crystal structures explain functional properties of two *E. coli* porins. Nature **358:**727-733.

24. **Crane, B. R., L. M. Siegel, and E. D. Getzoff.** 1995. Sulfite reductase structure at 1.6 A: evolution and catalysis for reduction of inorganic anions. Science **270:**59-67.

25. **Croal, L. R., Y. Jiao, and D. K. Newman.** 2007. The *fox* operon from *Rhodobacter* strain SW2 promotes phototrophic Fe(II) oxidation in *Rhodobacter capsulatus* SB1003. J. Bacteriol. **189:**1774-1782.

26. **Cross, A. R., J. F. Parkinson, and O. T. Jones.** 1985. Mechanism of the superoxide-producing oxidase of neutrophils. O_2 is necessary for the fast reduction of cytochrome *b*-245 by NADPH. Biochem. J. **226:**881-884.

27. **Cross, A. R., J. Rae, and J. T. Curnutte.** 1995. Cytochrome *b*-245 of the neutrophil superoxide-generating system contains two nonidentical hemes. J. Biol. Chem. **270:**17075-17077.

28. **Dancis, A., R. D. Klausner, A. G. Hinnebusch, and J. G. Barriocanal.** 1990. Genetic evidence that ferric reductase is required for iron uptake in *Saccharomyces cerevisiae*. Mol. Cell. Biol. **10:**2294-2301.

29. **Dancis, A., D. G. Roman, G. J. Anderson, A. G. Hinnebusch, and R. D. Klausner.** 1992. Ferric reductase of *Saccharomyces cerevisiae*: molecular characterization, role in iron uptake, and transcriptional control by iron. Proc. Natl. Acad. Sci. USA **89:**3869-3873.

30. **Dinauer, M. C., S. H. Orkin, R. Brown, A. J. Jesaitis, and C. A. Parkos.** 1987. The glycoprotein encoded by the X-linked chronic granulomatous disease locus is a component of the neutrophil cytochrome *b* complex. Nature **327:**717-720.

31. **Dodge, C. J., A. J. Francis, J. B. Gillow, G. P. Halada, C. Eng, and C. R. Clayton.** 2002. Association of uranium with iron oxides typically formed on corroding steel surfaces. Environ. Sci. Technol. **36:**3504-3511.

32. **Dugan, P. R., and D. G. Lundgren.** 1965. Energy supply for the chemoautotroph *Ferrobacillus ferrooxidans*. J. Bacteriol. **89:**825-834.

33. **Dunn, M. F., J. A. Ramirez-Trujillo, and I. Hernandez-Lucas.** 2009. Major roles of isocitrate lyase and malate synthase in bacterial and fungal pathogenesis. Microbiology **155:**3166-3175.

34. **Ehrenreich, A., and F. Widdel.** 1994. Anaerobic oxidation of ferrous iron by purple bacteria, a new type of phototrophic metabolism. Appl. Environ. Microbiol. **60:**4517-4526.

35. **Espejo, R. T., B. Escobar, E. Jedlicki, P. Uribe, and R. Badilla-Ohlbaum.** 1988. Oxidation of ferrous iron and elemental sulfur by *Thiobacillus ferrooxidans*. Appl. Environ. Microbiol. **54:**1694-1699.

36. **Finneran, K. T., M. E. Housewright, and D. R. Lovley.** 2002. Multiple influences of nitrate on uranium solubility during bioremediation of uranium-contaminated subsurface sediments. Environ. Microbiol. **4:**510-516.

37. **Fukami-Kobayashi, K., Y. Tateno, and K. Nishikawa.** 1999. Domain dislocation: a change of core structure in periplasmic binding proteins in their evolutionary history. J. Mol. Biol. **286:**279-290.

38. **Georgatsou, E., and D. Alexandraki.** 1994. Two distinctly regulated genes are required for ferric reduction, the first step of iron uptake in *Saccharomyces cerevisiae*. Mol. Cell. Biol. **14:**3065-3073.

39. **Gruez, A., D. Pignol, M. Zeghouf, J. Coves, M. Fontecave, J. L. Ferrer, and J. C. Fontecilla-Camps.** 2000. Four crystal structures of the 60 kDa flavoprotein monomer of the sulfite reductase indicate a disordered flavodoxin-like module. J. Mol. Biol. **299:**199-212.

40. **Hafenbradl, D., M. Keller, R. Dirmeier, R. Rachel, P. Rossnagel, S. Burggraf, H. Huber, and K. O. Stetter.** 1996. *Ferroglobus placidus* gen. nov., sp. nov., a novel hyperthermophilic archaeum that oxidizes Fe^{2+} at neutral pH under anoxic conditions. Arch. Microbiol. **166:**308-314.

41. **Halliwell, B., and J. M. Gutteridge.** 1984. Oxygen toxicity, oxygen radicals, transition metals and disease. Biochem. J. **219:**1-14.

42. **Hauck, S., M. Benz, A. Brune, and B. Schink.** 2001. Ferrous iron oxidation by denitrifying bacteria in profundal sediments of a deep lake (Lake Constance). FEMS Microbiol. Ecol. **37:**127-134.

43. **Hegler, F., N. R. Posth, J. Jiang, and A. Kappler.** 2008. Physiology of phototrophic iron(II)-oxidizing bacteria: implications for modern and ancient environments. FEMS Microbiol. Ecol. **66:**250-260.

44. **Heising, S., and B. Schink.** 1998. Phototrophic oxidation of ferrous iron by a *Rhodomicrobium vannielii* strain. Microbiology **144 (8):**2263-2269.

45. **Hintz, M. J., D. M. Mock, L. L. Peterson, K. Tuttle, and J. A. Peterson.** 1982. Equilibrium and kinetic studies of the interaction of cytochrome *P*-450cam and putidaredoxin. J. Biol. Chem. **257:**14324-14332.

46. **Holmquist, M.** 2000. Alpha/beta-hydrolase fold enzymes: structures, functions and mechanisms. Curr. Protein. Pept. Sci. **1:**209-235.

47. **Hubbard, P. A., A. L. Shen, R. Paschke, C. B. Kasper, and J. J. Kim.** 2001. NADPH-cytochrome *P*450 oxidoreductase. J. Biol. Chem. **276:**29163-29170.

48. **Jiao, Y., and D. K. Newman.** 2007. The *pio* operon is essential for phototrophic Fe(II) oxidation in *Rhodopseudomonas palustris* TIE-1. J. Bacteriol. **189:**1765-1773.

49. **Kappler, A., B. Schink, and D. K. Newman.** 2005. Fe(III) mineral formation and cell encrustation by the nitrate-dependent Fe(II)-oxidizer strain BoFeN1. Geobiology **3:**235-245.

50. **Kim, E. H., D. H. Nies, M. M. McEvoy, and C. Rensing.** 2011. Switch or funnel: how RND-type transport systems control periplasmic metal homeostasis. J. Bacteriol. **193:**2381-2387.

51. **Kondrashov, F. A., E. V. Koonin, I. G. Morgunov, T. V. Finogenova, and M. N. Kondrashova.** 2006. Evolution of glyoxylate cycle enzymes in metazoa: evidence of multiple horizontal transfer events and pseudogene formation. Biol. Direct **1:**31.

52. **Konhauser, K. O.** 2006. Bacterial iron biomineralisation in nature. FEMS Microbiol. Rev. **20:**315-326.

53. **Konhauser, K. O., T. Hamade, R. Raiswell, R. C. Morris, F. G. Ferris, G. Southam, and D. E. Canfield.** 2002. Could bacteria have formed the precambrian banded iron formations? Geology **30:**1079-1082.

54. **Konhauser, K. O., A. Kappler, and E. E. Roden.** 2011. Iron in microbial metabolisms. Elements **7:**89-93.

55. **Kumar, A., and H. P. Schweizer.** 2005. Bacterial resistance to antibiotics: active efflux and reduced uptake. Adv. Drug Deliv. Rev. **57:**1486-1513.

56. **Lack, J. G., S. K. Chaudhuri, R. Chakraborty, L. A. Achenbach, and J. D. Coates.** 2002. Anaerobic biooxidation of Fe(II) by *Dechlorosoma suillum*. Microb. Ecol. **43:**424-431.

57. **Lack, J. G., S. K. Chaudhuri, S. D. Kelly, K. M. Kemner, S. M. O'Connor, and J. D. Coates.** 2002. Immobilization of radionuclides and heavy metals through anaerobic bio-oxidation of Fe(II). Appl. Environ. Microbiol. **68:**2704-2710.

58. **Legatzki, A., S. Franke, S. Lucke, T. Hoffmann, A. Anton, D. Neumann, and D. H. Nies.** 2003. First step towards a quantitative model describing Czc-mediated heavy metal resistance in *Ralstonia metallidurans*. Biodegradation **14:**153-168.

59. **Li, X. Z., and H. Nikaido.** 2009. Efflux-mediated drug resistance in bacteria: an update. Drugs **69:**1555-1623.

60. **Lloyd, J. R., and J. C. Renshaw.** 2005. Bioremediation of radioactive waste: radionuclide-microbe interactions in laboratory and field-scale studies. Curr. Opin. Biotechnol. **16:**254-260.

61. **Lloyd, J. R., and J. C. Renshaw.** 2005. Microbial transformations of radionuclides: fundamental mechanisms and biogeochemical implications. Met. Ions Biol. Syst. **44:**205-240.

62. **Lorenz, M. C., and G. R. Fink.** 2002. Life and death in a macrophage: role of the glyoxylate cycle in virulence. Eukaryot. Cell **1:**657-662.

63. **Loschi, L., S. J. Brokx, T. L. Hills, G. Zhang, M. G. Bertero, A. L. Lovering, J. H. Weiner, and N. C. Strynadka.** 2004. Structural and biochemical identification of a novel bacterial oxidoreductase. J. Biol. Chem. **279:**50391-50400.

64. **Lovley, D. R.** 2000. Fe(III) and Mn(IV) reduction, p. 3-31. *In* D. R. Lovley (ed.), Environmental Microbe-Metal Interactions. ASM Press, Washington,DC.

65. **Lu, G., W. H. Campbell, G. Schneider, and Y. Lindqvist.** 1994. Crystal structure of the FAD-containing fragment of corn nitrate reductase at 2.5 A resolution: relationship to other flavoprotein reductases. Structure **2:**809-821.

66. **Ma, D., D. N. Cook, J. E. Hearst, and H. Nikaido.** 1994. Efflux pumps and drug resistance in gram-negative bacteria. Trends Microbiol. **2:**489-493.

67. **Madigan, M. T., J. M. Martinko, and T. D. Brock.** 2006. Brock Biology of Microorganisms, 11th ed. Pearson Prentice Hall, Upper Saddle River, NJ.

68. **Maturana, A., S. Arnaudeau, S. Ryser, B. Banfi, J. P. Hossle, W. Schlegel, K. H. Krause, and N. Demaurex.** 2001. Heme histidine ligands within gp91(phox) modulate proton conduction by the phagocyte NADPH oxidase. J. Biol. Chem. **276:**30277-30284.

69. **Mayhew, S. G., and M. L. Ludwig.** 1975. The enzymes. *In* P. D. Boyer (ed.), Flavodoxins and Electron-Transferring Flavoproteins, vol. 12B. Academic Press, Inc., New York.

70. **Miot, J., K. Benzerara, G. Morin, A. Kappler, S. Bernard, M. Obst, C. Férard, F. Skouri-Panet, J.-M. Guigner, N. Posth, M. Galvez, G. E. B. Jr., and F. Guyot.** 2009. Iron biomineralization by anaerobic neutrophilic iron-oxidizing bacteria. Geochim. Cosmochim. Ac. **73:**696-711.

71. **Muehe, E. M., S. Gerhardt, B. Schink, and A. Kappler.** 2009. Ecophysiology and the energetic benefit of mixotrophic Fe(II) oxidation by various strains of nitrate-reducing bacteria. FEMS Microbiol. Ecol. **70:**335-343.

72. **Nakayama, M., T. Akashi, and T. Hase.** 2000. Plant sulfite reductase: molecular structure, catalytic function and interaction with ferredoxin. J. Inorg. Biochem. **82:**27-32.

73. **Nardini, M., and B. W. Dijkstra.** 1999. Alpha/beta hydrolase fold enzymes: the family keeps growing. Curr. Opin. Struct. Biol. **9:**732-737.

74. **Neilands, J. B.** 1982. Microbial envelope proteins related to iron. Ann. Rev. Microbiol. **36:**285-309.

75. **Nielsen, J. L., and P. H. Nielsen.** 1998. Microbial nitrate-dependent oxidation of ferrous iron in activated sludge. Environ. Sci. Technol. **32:**3556-3561.

76. **Nies, D. H.** 1995. The cobalt, zinc, and cadmium efflux system CzcABC from *Alcaligenes eutrophus* functions as a cation-proton antiporter in *Escherichia coli*. J. Bacteriol. **177:**2707-2712.

77. **Nies, D. H.** 2003. Efflux-mediated heavy metal resistance in prokaryotes. FEMS Microbiol. Rev. **27:**313-339.

78. **Nies, D. H., and S. Silver.** 1995. Ion efflux systems involved in bacterial metal resistances. J. Ind. Microbiol. **14:**186-199.

79. **Nies, D. H., and S. Silver.** 1989. Plasmid-determined inducible efflux is responsible for resistance to cadmium, zinc, and cobalt in *Alcaligenes eutrophus*. J. Bacteriol. **171:**896-900.

80. **Nikaido, H.** 2003. Molecular basis of bacterial outer membrane permeability revisited. Microbiol. Mol. Biol. Rev. **67:**593-656.

81. **Nikaido, H., and Y. Takatsuka.** 2009. Mechanisms of RND multidrug efflux pumps. Biochimi. Biophys. Acta **1794:**769-781.

82. **Nikaido, H., and H. I. Zgurskaya.** 1999. Antibiotic efflux mechanisms. Curr. Opin. Infect. Dis. **12:**529-536.

83. **Nogues, I., I. Perez-Dorado, S. Frago, C. Bittel, S. G. Mayhew, C. Gomez-Moreno, J. A. Hermoso, M. Medina, N. Cortez, and N. Carrillo.** 2005. The ferredoxin-NADP(H) reductase from *Rhodobacter capsulatus*: molecular structure and catalytic mechanism. Biochemistry **44:**11730-11740.

84. **Osborn, M. J., and H. C. Wu.** 1980. Proteins of the outer membrane of gram-negative bacteria. Ann. Rev. Microbiol. **34:**369-422.

85. **Osborne, C., L. M. Chen, and R. G. Matthews.** 1991. Isolation, cloning, mapping, and nucleotide sequencing of the gene encoding flavodoxin in *Escherichia coli*. J. Bacteriol. **173:**1729-1737.

86. **Papanikolaou, G., and K. Pantopoulos.** 2005. Iron metabolism and toxicity. Toxicol. Appl. Pharmacol. **202:**199-211.

87. **Pfaffl, M. W.** 2001. A new mathematical model for relative quantification in real-time RT-PCR. Nucl. Acids Res. **29:**e45.

88. **Popov, V. N., E. A. Moskalev, M. Shevchenko, and A. T. Eprintsev.** 2005. Comparative analysis of the glyoxylate cycle clue enzyme isocitrate lyases from organisms of different systemic groups. Zh. Evol. Biokhim. Fiziol. **41:**507-513.

89. **Ramirez, P., N. Guiliani, L. Valenzuela, S. Beard, and C. A. Jerez.** 2004. Differential protein expression during growth of *Acidithiobacillus ferrooxidans* on ferrous iron, sulfur compounds, or metal sulfides. Appl. Environ. Microbiol. **70:**4491-4498.

90. **Rensing, C., T. Pribyl, and D. H. Nies.** 1997. New functions for the three subunits of the CzcCBA cation-proton antiporter. J. Bacteriol. **179:**6871-6879.

91. **Roman, D. G., A. Dancis, G. J. Anderson, and R. D. Klausner.** 1993. The fission yeast ferric reductase gene frp1+ is required for ferric iron uptake and encodes a protein that is homologous to the gp91-phox subunit of the human NADPH phagocyte oxidoreductase. Mol. Cell. Biol. **13:**4342-4350.

92. **Roome, P. W., Jr., J. C. Philley, and J. A. Peterson.** 1983. Purification and properties of putidaredoxin reductase. J. Biol. Chem. **258:**2593-2598.

93. **Rotrosen, D., C. L. Yeung, and J. P. Katkin.** 1993. Production of recombinant cytochrome *b*558 allows reconstitution of the phagocyte NADPH oxidase solely from recombinant proteins. J. Biol. Chem. **268:**14256-14260.

94. **Rotrosen, D., C. L. Yeung, T. L. Leto, H. L. Malech, and C. H. Kwong.** 1992. Cytochrome *b*558: the flavin-binding component of the phagocyte NADPH oxidase. Science **256:**1459-1462.

95. **Salton, M. R. J., and K. S. Kim.** 1996. Medical Microbiolgy. *In* S. Baron (ed.), Chapter 2, Structure, 4th ed. The University of Texas Medical Branch at Galveston, Galveston, TX.

96. **Sani, R. K., B. M. Peyton, A. Dohnalkova, and J. E. Amonette.** 2005. Reoxidation of reduced uranium with iron(III) hydroxides under sulfate-reducing conditions. Environ. Sci. Technol. **39:**2059-2066.

97. **Schnaitman, C. A., M. S. Korczynski, and D. G. Lundgren.** 1969. Kinetic studies of iron oxidation by whole cells of *Ferrobacillus ferrooxidans*. J. Bacteriol. **99:**552-557.

98. **Segal, A. W., I. West, F. Wientjes, J. H. Nugent, A. J. Chavan, B. Haley, R. C. Garcia, H. Rosen, and G. Scrace.** 1992. Cytochrome *b*-245 is a flavocytochrome containing FAD and the NADPH-binding site of the microbicidal oxidase of phagocytes. Biochem. J. **284:**781-788.

99. **Sharma, V., S. Sharma, K. Hoener zu Bentrup, J. D. McKinney, D. G. Russell, W. R. Jacobs, Jr., and J. C. Sacchettini.** 2000.

Structure of isocitrate lyase, a persistence factor of *Mycobacterium tuberculosis*. Nat. Struct. Biol. **7:**663-668.

100. **Skovran, E., and D. M. Downs.** 2003. Lack of the ApbC or ApbE protein results in a defect in Fe-S cluster metabolism in *Salmonella enterica* serovar Typhimurium. J. Bacteriol. **185:**98-106.
101. **Straub, K. L., M. Benz, B. Schink, and F. Widdel.** 1996. Anaerobic, nitrate-dependent microbial oxidation of ferrous iron. Appl. Environ. Microbiol. **62:**1458-1460.
102. **Straub, K. L., F. A. Rainey, and F. Widdel.** 1999. *Rhodovulum iodosum* sp. nov. and *Rhodovulum robiginosum* sp. nov., two new marine phototrophic ferrous-iron-oxidizing purple bacteria. Int. J. Syst. Bacteriol. **49:**729-735.
103. **Sugio, T., C. Domatsu, O. Munakata, T. Tano, and K. Imai.** 1985. Role of a ferric ion-reducing system in sulfur oxidation of *Thiobacillus ferrooxidans*. Appl. Environ. Microbiol. **49:**1401-1406.
104. **Sugio, T., K. Wada, M. Mori, K. Inagaki, and T. Tano.** 1988. Synthesis of an iron-oxidizing system during growth of *Thiobacillus ferrooxidans* on sulfur-basal salts medium. Appl. Environ. Microbiol. **54:**150-152.
105. **Taha, T. M., T. Kanao, F. Takeuchi, and T. Sugio.** 2008. Reconstitution of iron oxidase from sulfur-grown *Acidithiobacillus ferrooxidans*. Appl. Environ. Microbiol. **74:**6808-6810.

106. **Tam, R., and M. H. Saier, Jr.** 1993. Structural, functional, and evolutionary relationships among extracellular solute-binding receptors of bacteria. Microbiol. Rev. **57:**320-346.

107. **Teahan, C., P. Rowe, P. Parker, N. Totty, and A. W. Segal.** 1987. The X-linked chronic granulomatous disease gene codes for the beta-chain of cytochrome *b*-245. Nature **327:**720-721.

108. **Touati, D.** 2000. Iron and oxidative stress in bacteria. Arch. Biochem. Biophys. **373:**1-6.

109. **Tu, S. C., J. E. Becvar, and J. W. Hastings.** 1979. Kinetic studies on the mechanism of bacterial NAD(P)H:flavin oxidoreductase. Arch. Biochem. Biophys. **193:**110-116.

110. **Vandesompele, J., K. De Preter, F. Pattyn, B. Poppe, N. Van Roy, A. De Paepe, and F. Speleman.** 2002. Accurate normalization of real-time quantitative RT-PCR data by geometric averaging of multiple internal control genes. Gen. Biol. **3:**RESEARCH0034.

111. **Wall, J. D., and L. R. Krumholz.** 2006. Uranium reduction. Ann. Rev. Microbiol. **60:**149-166.

112. **Walter, M., T. Arnold, T. Reich, and G. Bernhard.** 2003. Sorption of uranium(VI) onto ferric oxides in sulfate-rich acid waters. Environ. Sci. Technol. **37:**2898-2904.

113. **Webb, E. A., J. W. Moffett, and J. B. Waterbury.** 2001. Iron stress in open-ocean cyanobacteria (*Synechococcus*, *Trichodesmium*, and

Crocosphaera spp.): identification of the IdiA protein. Appl. Environ. Microbiol. **67:**5444-5452.

114. **Weber, K. A., L. A. Achenbach, and J. D. Coates.** 2006. Microorganisms pumping iron: anaerobic microbial iron oxidation and reduction. Nat. Rev. Microbiol. **4:**752-764.

115. **Weber, K. A., D. B. Hedrick, A. D. Peacock, J. C. Thrash, D. C. White, L. A. Achenbach, and J. D. Coates.** 2009. Physiological and taxonomic description of the novel autotrophic, metal oxidizing bacterium, *Pseudogulbenkiania* sp. strain 2002. Appl. Microbiol. Biotechnol. **83:**555-565.

116. **Weber, K. A., F. W. Picardal, and E. E. Roden.** 2001. Microbially catalyzed nitrate-dependent oxidation of biogenic solid-phase Fe(II) compounds. Environ. Sci. Technol. **35:**1644-1650.

117. **Weber, K. A., J. Pollock, K. A. Cole, S. M. O'Connor, L. A. Achenbach, and J. D. Coates.** 2006. Anaerobic nitrate-dependent iron(II) bio-oxidation by a novel lithoautotrophic betaproteobacterium, strain 2002. Appl. Environ. Microbiol. **72:**686-694.

118. **Widdel, F., S. Schnell, S. Heising, A. Ehrenreich, B. Assmus, and B. Schink.** 1993. Ferrous iron oxidation by anoxygenic phototrophic bacteria. Nature **362:**834-836.

119. **Wosten, M. M., L. F. Kox, S. Chamnongpol, F. C. Soncini, and E. A. Groisman.** 2000. A signal transduction system that responds to extracellular iron. Cell **103:**113-125.

120. **Yarzabal, A., G. Brasseur, J. Ratouchniak, K. Lund, D. Lemesle-Meunier, J. A. DeMoss, and V. Bonnefoy.** 2002. The high-molecular-weight cytochrome *c* Cyc2 of *Acidithiobacillus ferrooxidans* is an outer membrane protein. J. Bacteriol. **184:**313-317.

121. **Yu, L., M. T. Quinn, A. R. Cross, and M. C. Dinauer.** 1998. Gp91(phox) is the heme binding subunit of the superoxide-generating NADPH oxidase. Proc. Natl. Acad. Sci. USA **95:**7993-7998.

122. **Yu, L., L. Zhen, and M. C. Dinauer.** 1997. Biosynthesis of the phagocyte NADPH oxidase cytochrome *b*558. Role of heme incorporation and heterodimer formation in maturation and stability of gp91phox and p22phox subunits. J. Biol. Chem. **272:**27288-27294.

123. **Zgurskaya, H. I.** 2002. Molecular analysis of efflux pump-based antibiotic resistance. Int. J. Med. Microbiol. **292:**95-105.

124. **Zgurskaya, H. I., and H. Nikaido.** 2000. Multidrug resistance mechanisms: drug efflux across two membranes. Mol. Microbiol. **37:**219-225.

Section 2

1. **Achenbach, L. A., U. Michaelidou, R. A. Bruce, J. Fryman, and J. D. Coates.** 2001. *Dechloromonas agitata* gen. nov., sp. nov. and *Dechlorosoma suillum* gen. nov., sp. nov., two novel environmentally dominant (per)chlorate-reducing bacteria and their phylogenetic position. Int. J. Syst. Evol. Microbiol. **51:**527-533.
2. **Anbar, M., S. Guttmann, and Z. Lewitus.** 1959. The mode of action of perchlorate ions on the iodine uptake of the thyroid gland. Int. J. Appl. Radiat. Isot. **7:**87-96.
3. **Balk, M., T. van Gelder, S. A. Weelink, and A. J. Stams.** 2008. (Per)chlorate reduction by the thermophilic bacterium *Moorella perchloratireducens* sp. nov., isolated from underground gas storage. Appl. Environ. Microbiol. **74:**403-409.
4. **Baneyx, F., and M. Mujacic.** 2004. Recombinant protein folding and misfolding in *Escherichia coli*. Nat. Biotechnol. **22:**1399-1408.
5. **Bender, K. S., C. Shang, R. Chakraborty, S. M. Belchik, J. D. Coates, and L. A. Achenbach.** 2005. Identification, characterization, and classification of genes encoding perchlorate reductase. J. Bacteriol. **187:**5090-5096.
6. **Bruce, R. A., L. A. Achenbach, and J. D. Coates.** 1999. Reduction of (per)chlorate by a novel organism isolated from paper mill waste. Environ. Microbiol. **1:**319-329.

7. **Chaudhuri, S. K., J. G. Lack, and J. D. Coates.** 2001. Biogenic magnetite formation through anaerobic biooxidation of Fe(II). Appl. Environ. Microbiol. **67:**2844-2848.

8. **Chaudhuri, S. K., S. M. O'Connor, R. L. Gustavson, L. A. Achenbach, and J. D. Coates.** 2002. Environmental factors that control microbial perchlorate reduction. Appl. Environ. Microbiol. **68:**4425-4430.

9. **Coates, J. D., and L. A. Achenbach.** 2004. Microbial perchlorate reduction: rocket-fueled metabolism. Nat. Rev. Microbiol. **2:**569-580.

10. **Coates, J. D., R. Chakraborty, J. G. Lack, S. M. O'Connor, K. A. Cole, K. S. Bender, and L. A. Achenbach.** 2001. Anaerobic benzene oxidation coupled to nitrate reduction in pure culture by two strains of *Dechloromonas*. Nature **411:**1039-1043.

11. **Coates, J. D., K. A. Cole, R. Chakraborty, S. M. O'Connor, and L. A. Achenbach.** 2002. Diversity and ubiquity of bacteria capable of utilizing humic substances as electron donors for anaerobic respiration. Appl. Environ. Microbiol. **68:**2445-2452.

12. **Coates, J. D., U. Michaelidou, R. A. Bruce, S. M. O'Connor, J. N. Crespi, and L. A. Achenbach.** 1999. Ubiquity and diversity of dissimilatory (per)chlorate-reducing bacteria. Appl. Environ. Microbiol. **65:**5234-5241.

13. **Frankel, S., R. Sohn, and L. Leinwand.** 1991. The use of sarkosyl in generating soluble protein after bacterial expression. Proc. Natl. Acad. Sci. USA **88:**1192-1196.

14. **Greer, M. A., G. Goodman, R. C. Pleus, and S. E. Greer.** 2002. Health effects assessment for environmental perchlorate contamination: the dose response for inhibition of thyroidal radioiodine uptake in humans. Environ. Health Persp. **110:**927-937.

15. **Hatzinger, P. B.** 2005. Perchlorate biodegradation for water treatment. Environ. Sci. Technol. **39:**239A-247A.

16. **Heinnickel, M., S. C. Smith, J. Koo, S. M. O'Connor, and J. D. Coates.** 2011. A bioassay for the detection of perchlorate in the ppb range. Environ. Sci. Technol. **45:**2958-2964.

17. **Jormakka, M., D. Richardson, B. Byrne, and S. Iwata.** 2004. Architecture of NarGH reveals a structural classification of Mo-bisMGD enzymes. Structure **12:**95-104.

18. **Kengen, S. W., G. B. Rikken, W. R. Hagen, C. G. van Ginkel, and A. J. Stams.** 1999. Purification and characterization of (per)chlorate reductase from the chlorate-respiring strain GR-1. J. Bacteriol. **181:**6706-6711.

19. **Koester, C. J., H. R. Beller, and R. U. Halden.** 2000. Analysis of perchlorate in groundwater by electrospray ionization mass

spectrometry/mass spectrometry. Environ. Sci. Technol. **34:**1862-1864.

20. **Lack, J. G., S. K. Chaudhuri, R. Chakraborty, L. A. Achenbach, and J. D. Coates.** 2002. Anaerobic biooxidation of Fe(II) by *Dechlorosoma suillum*. Microb. Ecol. **43:**424-431.

21. **LaVallie, E. R., E. A. DiBlasio-Smith, L. A. Collins-Racie, Z. Lu, and J. M. McCoy.** 2003. Thioredoxin and related proteins as multifunctional fusion tags for soluble expression in *E. coli*. Meth. Mol. Biol. **205:**119-140.

22. **Lawrence, J. E., S. H. Lamm, S. Pino, K. Richman, and L. E. Braverman.** 2000. The effect of short-term low-dose perchlorate on various aspects of thyroid function. Thyroid **10:**659-663.

23. **Leonardi, R., S. A. Fairhurst, M. Kriek, D. J. Lowe, and P. L. Roach.** 2003. Thiamine biosynthesis in *Escherichia coli*: isolation and initial characterization of the ThiGH complex. FEBS Lett. **539:**95-99.

24. **Logan, B. E.** 2001. Assessing the outlook for perchlorate remediation. Environ. Sci. Technol. **35:**482A-487A.

25. **Logan, B. E., J. Wu, and R. F. Unz.** 2001. Biological perchlorate reduction in high-salinity solutions. Water Res. **35:**3034-3038.

26. **Logan, B. E., H. Zhang, P. Mulvaney, M. G. Milner, I. M. Head, and R. F. Unz.** 2001. Kinetics of perchlorate- and chlorate-respiring bacteria. Appl. Environ. Microbiol. **67:**2499-2506.

27. **McEwan, A. G., J. P. Ridge, C. A. McDevitt, and P. Hugenholtz.** 2002. The DMSO reductase family of microbial molybdenum enzymes; molecular properties and role in the dissimilatory reduction of toxic elements. Geomicrobiol. J. **19:**3-21.

28. **Nerenberg, R., Y. Kawagoshi, and B. E. Rittmann.** 2006. Kinetics of a hydrogen-oxidizing, perchlorate-reducing bacterium. Water Res. **40:**3290-3296.

29. **O'Connor, S. M., and J. D. Coates.** 2002. Universal immunoprobe for (per)chlorate-reducing bacteria. Appl. Environ. Microbiol. **68:**3108-3113.

30. **Okeke, B. C., and W. T. Frankenberger, Jr.** 2003. Molecular analysis of a perchlorate reductase from a perchlorate-respiring bacterium Perc1ace. Microbiol. Res. **158:**337-344.

31. **Okeke, B. C., T. Giblin, and W. T. Frankenberger, Jr.** 2002. Reduction of perchlorate and nitrate by salt tolerant bacteria. Environ. Pollut. **118:**357-363.

32. **Okeke, B. C., G. Ma, Q. Cheng, M. E. Losi, and W. T. Frankenberger, Jr.** 2007. Development of a perchlorate reductase-based biosensor for real time analysis of perchlorate in water. J. Microbiol. Meth. **68:**69-75.

33. **Romanenko, V. I., V. N. Koren'kov, and S. I. Kuznetsov.** 1976. Bacterial decomposition of ammonium perchlorate. Mikrobiologiia **45:**204-209.

34. **Smith, H. E.** 2007. The transcriptional response of *Escherichia coli* to recombinant protein insolubility. J. Struct. Funct. Genomics **8:**27-35.

35. **Soldin, O. P., L. E. Braverman, and S. H. Lamm.** 2001. Perchlorate clinical pharmacology and human health: a review. Theor. Drug Monit. **23:**316-331.

36. **Sorensen, H. P., and K. K. Mortensen.** 2005. Advanced genetic strategies for recombinant protein expression in *Escherichia coli*. J. Biotechnol. **115:**113-128.

37. **Sorensen, H. P., and K. K. Mortensen.** 2005. Soluble expression of recombinant proteins in the cytoplasm of *Escherichia coli*. Microb. Cell Fact. **4:**1.

38. **Urbansky, E. T.** 2002. Perchlorate as an environmental contaminant. Environ. Sci. Pollut. Res. Int. **9:**187-192.

39. **Urbansky, E. T.** 2000. Perchlorate in the Environment. Kluwer Academic/Plenum Publishers, New York.

40. **Wolff, J.** 1998. Perchlorate and the thyroid gland. Pharmacol. Rev. **50:**89-105.

41. **Yoshimatsu, K., T. Iwasaki, and T. Fujiwara.** 2002. Sequence and electron paramagnetic resonance analyses of nitrate reductase NarGH

from a denitrifying halophilic euryarchaeote *Haloarcula marismortui*. FEBS letters **516:**145-150.

42. **Yu, X., C. Amrhein, M. A. Deshusses, and M. R. Matsumoto.** 2006. Perchlorate reduction by autotrophic bacteria in the presence of zero-valent iron. Environ. Sci. Technol. **40:**1328-1334.

43. **Zhang, H., M. A. Bruns, and B. E. Logan.** 2002. Perchlorate reduction by a novel chemolithoautotrophic, hydrogen-oxidizing bacterium. Environ. Microbiol. **4:**570-576.

VITA

Graduate School
Southern Illinois University

Ming Gao

Mingg0923@gmail.com

Wuhan University, Wuhan, China
Bachelor of Science, Biological Sciences, May 2006

Special Honors and Awards:

Dissertation Research Assistantship Award, Southern Illinois University Carbondale. (2009-2010)

Dissertation Title:

Identification and Analysis of Proteins and Genes Responsible for Microbial Anaerobic Nitrate-Dependent Iron Oxidation and Overexpression in *E. coli* of Perchlorate Reductase

Major Professor: Laurie Achenbach

Publications:

Ming Gao, and Laurie A. Achenbach. 2011. A Proteomics Approach to Identify Proteins and Genes Responsible for Anaerobic Nitrate-dependent Fe^{2+} Oxidation. (*Submitted*)